



INSTITUTO SUPERIOR TÉCNICO

INTEGRATOR PROJECT IN AEROSPACE ENGINEERING

Urban Air Mobility - Concept Design

Bologna Degree in Aerospace Engineering
Academic year 2021/2022

Group 8:

Afonso MAGALHÃES, Nº 95765
António LOPES, Nº 95771
Beatriz PEDROSO, Nº 95773
Diogo SOUSA, Nº 95779
Fábio MONTEIRO, Nº 95786
Francisco CARVALHO, Nº 95791
João MARTINS, Nº 95806
José LUCIANO, Nº 92702

Professors:
Afzal SULEMAN
Frederico AFONSO

Contents

1	Executive Summary	1
2	Introduction	1
3	Mission Overview	2
3.1	Objectives and motivation	2
3.2	Design requirements	2
3.3	Market Analysis	2
3.3.1	Market Study	3
3.3.2	Concept Study	3
4	Aircraft Configuration and Conceptual Design	5
4.1	Concept Design	5
4.1.1	Concept Design 1	6
4.1.2	Concept Design 2	6
4.1.3	Concept Design 3	6
4.1.4	Concept Design 4	7
4.1.5	Concept Design 5	7
4.1.6	Concept Design 6	8
4.2	Concept Choice	8
4.2.1	Powerplant	9
4.2.2	Stability	11
4.2.3	Efficiency	12
4.2.4	Dimensions	13
4.2.5	Concept Comparative Value	14
5	Aircraft Sizing and Design Point	15
5.1	Mission Profile	15
5.2	Maximum Take-off Weight Estimation - MTOW	17
5.3	Design Point for Fixed Wing and VTOL	18
5.3.1	Forward Flight Design Constrains	18
5.3.2	Vertical Flight Design Constrains	19
5.3.3	Design Point	20
6	Wing Design	21
6.1	Wing Main Dimensions	21
6.2	Airfoil Selection	21
6.3	Lift and Drag Estimation	23
6.4	Wing's Location	24
7	Tail Design	25
7.1	Tail Sizing	25
7.2	Airfoil Selection	26
7.3	Drag estimation	27

8 Propulsive System Design	28
8.1 Power Plant	28
8.2 Rotors	28
8.3 Minimum Power Required	30
8.3.1 VTOL	30
8.3.2 Cruise Flight	31
8.4 Components choice	33
8.4.1 Electric Motors	33
8.4.2 Internal Combustion Engine and Generator	34
8.4.3 Transmission and Gearbox	35
9 Fuselage Design	36
9.1 Volume Considerations	36
9.2 Emergency Exits Requirements	37
9.3 Landing Gear design	37
9.4 Aerodynamic Considerations	38
9.4.1 Fuselage Shape	38
9.4.2 Drag Estimation	39
10 Weight Distribution	40
11 Static Stability	42
11.1 Longitudinal Stability	42
11.2 Lateral Stability	43
11.3 Direction Stability	44
11.4 Vertical Stability	44
12 Aircraft Structures	45
12.1 V-n Diagram	45
12.2 Wing Structural Analysis	48
12.2.1 Lift Distribution	49
12.2.2 Wing Weight Distribution	49
12.2.3 Shear Force and Bending Moments	50
13 CAD Design	51
14 Pollutant and Noise Emissions Estimations	52
14.1 Pollutant Emissions	52
14.2 Noise Emissions	54
15 Conclusion	54
15.1 Possible Improvements	54
15.2 Final Remarks	55
References	56

List of Figures

1	Bell Nexus 6HX. [3]	4
2	Rolls-Royce EVTOL. [23]	4
3	Uber Elevate eCRM-001. [36]	4
4	Archer Maker. [18]	4
5	Lilium Jet. [16]	5
6	Eve. [11]	5
7	Concept design 1	6
8	Concept design 2	6
9	Concept design 3	7
10	Concept Design 4	7
11	Concept Design 5	8
12	Concept Design 6	8
13	Criterion Diagram	9
14	Visualization of the final concept.	15
15	Major cities in the city of Japan in which the service will be conducted.	16
16	Plot of our mission profile.	17
17	Mass distribution for an aircraft. [12]	18
18	Parametric analysis of the payload energy specific density and cruise speed	20
19	Historical trends for Wing Design.[28]	21
20	Comparison of the 6 NACA airfoils	22
21	NACA 4412	23
22	Possible tail shapes and configurations.[26]	25
23	Volume Coefficient historical values.[26]	25
24	Historical values for taper and aspect ratio.[26]	26
25	Comparison of the NACA 0009 and NACA 0012 for the Horizontal Tail	26
26	Comparison of the NACA 0009 and NACA 0012 for the Vertical Tail	27
27	Power Plant Evolution	28
28	$\frac{C_T}{C_P}$ as a function of C_P (three-blade propeller, $C_L = 0.5$, AF=100) [6]	31
29	Thrust and efficiency correction factor for different numbers of rotor blades [6]	31
30	C_P as a function of J , η_P , and blade pitch at 75% of its length, $\theta_{3/4}$ (three-blade propeller, $C_L = 0.5$, AF=100) [6]	32
31	APM120 [8]	34
32	LTS101-850B-2 [17]	35
33	Honeywell generator [13]	35
34	Fuselage cross-section.	36
35	Emergency exit required for passenger transpot aircraft by FAR 25.807 for <i>Type II</i> .	37
36	CAD model of the landing skid	38
37	C_{D_0} as a function of the fuselage fineness ratio.	38
38	Sketch of the fuselage shape. The first sketch is a side view and the second is a top view.	39
39	Graphic visualization of the fuselage interior, showing the components distribution.	41
40	Graphic representation of the lift forces on the wing and horizontal tail.	42
41	Graphics showing the changes of ϵ_α .	43
42	Example of a V-n diagram	46
43	Typical values for the gust velocities [6]	47
44	Flight Envelope and Gust Envelope	48
45	Example of Loads in Lifting Surfaces	48
46	Evolution of the shear force across half of the wing	50

47	Evolution of the bending moment across half of the wing	51
48	Model Render	51
49	Isometric view	52
50	Top view	52
51	Side view	52
52	Front view	52

List of Tables

1	Characteristics of some concepts already developed.	5
2	Characteristics of some concepts already developed.	5
3	Relative main criterion punctuation.	9
4	Powerplant subcriteria relative scores.	10
5	Cruise speed relative scores.	10
6	Maximum range relative scores.	10
7	Maximum power installed relative scores.	10
8	Air emissions relative scores.	11
9	Noise emissions relative scores.	11
10	Pollution subcriteria mean scores	11
11	Powerplant subcriteria mean scores.	11
12	Stability relative scores.	12
13	Efficiency Subcriteria relative scores	12
14	Efficiency mean scores	12
15	Efficiency in hover relative scores.	13
16	Efficiency in cruise relative scores.	13
17	Dimensions subcriteria relative scores.	13
18	Comfort relative scores.	13
19	External dimensions relative scores.	14
20	Dimensions mean scores.	14
21	Analytical Hierarchy Process end results	14
22	Chosen cities to implement the project and the distance between them and the capital of Japan.	15
23	Mission segment's characterization.	16
24	Mass distribution throughout the components of our aircraft.	18
25	Comparison of some properties for the NACA 2412 and NACA 4412 airfoils	23
26	Tail	27
27	Vertical tail	27
28	Horizontal tail	27
29	Rotor Area and Radius for single and coaxial rotors	29
30	Power needed per Rotor for single and coaxial rotors	30
31	Total power for single and coaxial rotors	30
32	Electric motors and respective specifications [1][2][7][8][34]	34
33	Turboshaft engines and respective specifications [5][9][10][22]	34
34	Generator specifications [13]	35
35	Passengers compartment requirements and chosen values.	36
36	Dimensions for a <i>Type II</i> emergency exit door.	37
37	Longitudinal center of gravity position of each components. The distances are measured from the front of the nose of the fuselage.	40
38	Parameters for the V-n diagram calculations	45
39	Relevant velocities (m/s) for the V-n diagram	46
40	Gust Velocities	47
41	Load factors accounting with the gust loads	47

1 Executive Summary

The project developed during this second semester consists in the conceptual design of a VTOL aircraft in the context of Urban Air Mobility (UAM) that could conduct different missions. This report describes the final decisions taken and also the entire thought process done in the development of the work, with difficulties and solutions also documented. Simultaneously and throughout the development of this work, the requirements need to always be kept in mind and respected.

2 Introduction

As previously mentioned, the aim of this report is to explain and provide the full analysis of the creating process of an hybrid Urban Air Mobility (UAM) aircraft. As so, this development was sub-categorized in diverse sections, so that the process was the most organized and well achieved possible.

To begin with, a mission overview, discussed in section 3, was conducted in order to define not only the motivation, but also the design requirements that must be met by the aircraft. Moreover, in section 3.3, an analysis on the market, in which the UAM was going to operate, was also carried out. Hence, the group decided the mission purpose, in 3.3.1, and evaluated some competitor models, which are being developed in the industry of UAM and will be available in the market in the upcoming years, considered in section 3.3.2.

Then, the aircraft design and the conceptual design commenced, analyzed in section 4. With the information gathered, the group designed different concepts and compared them in light of many criteria considered important, in order to choose the most suitable one.

Furthermore, section 5 is focused on defining the mission profile and determining the first design point. Such was performed with basis in various estimated values, marking the beginning of the iterative process with the initial sizing. In addition, an estimation of the MTOW was computed in section 5.2.

On section 6 and 7, the airfoils of the aerodynamic surfaces were selected and drag and lift studies on the wings were conducted.

On top of that, the propulsive system was also addressed. Thus, taking into consideration the mission profile and the requirements set, the power plant was defined and presented in section 8.1. The rotors also undergone a tight examination, which is described in section 8.2.

Moreover, the design of the fuselage, in section 9 is also accounted for. Several considerations on volume, aerodynamics, emergency exits requirements, landing gear design and drag estimation were made.

On section 10, a study on weight distribution was done, which was crucial for the computation of the static margin. The static stability was also assessed in section 11.

It is also to be highlighted that section 12 has as main objective the description and analysis of the structural loads that the aircraft is going to subjected to. The V-n diagram was, then, represented and a wing structural analysis was performed.

Finally, both pollutant and noise emissions estimations were calculated and presented in section 14. A MATLAB program, provided in the classes, proved to be useful to do so.

So that the full concept could be well visualized, a CAD model was designed, which is shown in section 13.

The Aircraft Design Tool, made available by the professors, was of great use and played a massive part on the project, by aiding the computation of the design points, mass estimation and the aerodynamic performance of the aircraft.

3 Mission Overview

3.1 Objectives and motivation

Every day new concepts rise which contribute to improving the quality of life of the population in general. The world of mobility and transport is no exception, with the desire to transport passengers in safer, faster, greener, and more innovative ways. The concept of Urban Air Mobility arises naturally, pushing the industry to reinvent the way humans commute everyday.

The Vertical Take-Off and Landing (VTOL) vehicles are considered to have a high versatility since they don't require a long runaway to take-off or landing, only a small helipad. This allows to:

- Increase mobility and reduce commuting times in highly populated cities (acting as an “air taxi”);
- Expand the accessibility of cargo delivery systems and reduce their times;
- Increase accessibility and reduce operation times for civil protection operations.

These operations are currently performed by helicopters in a small scale due to major limitations, such as high noise emissions, high energy and power requirements, as well as short range distance. Therefore, in order to ensure these needs, by improving performance and complying with both the market demand and environmental regulations, a new generation of eVTOL aircraft appears.

3.2 Design requirements

This project's main goal is to design an innovative hybrid-electric VTOL for Urban Air Mobility to start to operate in 2030 for tourism tours or/and provide itineraries in Tokyo, Japan.

The initial design requirements were the following. Some aspects were slightly changed throughout the project development.

- Payload of 80 kg
- Operational radius - 200 to 300 km
- Cruise speed - Approximately 300km/h
- Propulsion - Hybrid-electric
- Types and numbers of engines - open to design

3.3 Market Analysis

Prior to the start of the concept design of an aircraft, it is crucial to understand the market in which it will be introduced. Thus, as UAM is an emerging aviation market that seeks to revolutionize mobility around metropolitan areas, searching for existing competitors in the market, evaluating the readiness of a certain region to accept such a transportation system, and defining the main mission the aircraft has to perform are three of the main topics to take into consideration in this situation.

The following subsections (3.3.1 and 3.3.2) will focus on the market study and the concept study that was performed before commencing the concept design.

3.3.1 Market Study

UAM envisions a safe and efficient aviation transportation system that will use highly automated aircraft and will operate at lower altitudes within urban and suburban areas. Thus, it is a recent and growing industry that may be the solution major cities need to turn the time consuming commutes to work into a more comfortable, time-efficient and safe travel. Yet, there are several other missions that have been proposed in the past to tackle challenges in dense and congested cities. Hence, other publicly stated missions in the UAM space comprise airport shuttles to provide faster connectivity for airline passengers to/from existing airports, end-to-end city transfer, allowing passengers to bypass city traffic and rapidly move from one side of the city to the other, and “metro-like” services to connect passengers to other existing forms of mass transit.

Furthermore, before UAM can be fully developed, some technological and infrastructural concerns need to be overcome, and many regulatory issues need to be addressed. In addition, every city has a different level of development and a distinct market. Thus, both the type of mission and the concept choice are greatly impacted by the region it is designed for. As so, a market study was conducted.

Initially, the group agreed that the recurrent situation of the long drives of commuting to work should be the first problem to be tackled. Hence, the study began by listing the cities in which it takes the most time to get to work. Beijing, Tokyo, New York and Vancouver ended up to be the group’s main focus. It was also decided that the city of Lisbon would be examined, because of the proximity the group has with it. For each region, a research on the monthly average salary of the country and on the price, trips frequency, and time it takes to get to the city centre by the means of transportation available was conducted.

To begin with, even though the transfers between Cascais, Sintra, the South Margin of Lisbon and the *Parque das Nações* region were of major importance, the group ruled out this option since the mission range would be of around 30 to 50 km, which is a rather low value. The business people working in the enterprises located in *Parque das Nações* region would afford such trips in the aircraft. Nevertheless, there are plenty of other options to get them to work.

From the remaining cities, we acknowledged that Tokyo was on top of the list of most problematic zones. In fact, during the morning rush hours, the traffic volume on certain urban and suburban trains is so intense that passengers are pressed against each other to a degree in which they are unable to move. On top of that, Japan is a luxurious market, given the monthly average salary, which is an advantage in the beginning, to get the development costs covered. In fact, it could materialize into a profitable market due to the standard of living of some of its population. Furthermore, this city is the one that has the most helipads in the whole world, which means that the infrastructure is fully prepared to have UAM installed.

Thus, after this analysis, the market was narrowed to the city of Tokyo.

Furthermore, Tokyo and the cities that surround it share a lot of business. And, if the people that inhabit and work in a city, other than Japan’s capital, want to get to the centre of Tokyo, they need to take several means of transportation (some of them quite busy) or take their private car, which would not only take a lot of time but would also be very exhausting.

As so, the group is designing an aircraft, whose mission is to transport passengers from the surrounding cities of Japan’s capital to the centre of Tokyo. For the reasons mentioned above, this option seemed the most viable one.

3.3.2 Concept Study

Bearing in mind the mission requirements presented in section 3.2 and the market study, which was assessed in section 3.3.1, some research was conducted in order to find some competitor models, which are being developed in the industry of UAM and will be on the market in the upcoming years. This allowed us to compare some characteristics and configurations, and decide which granted the

most advantages and fulfilled the pre-requisites already discussed. Hence, this study is fundamental to estimate parameters for the aircraft design.

Figures 1, 2, 3, 4, 5 and 6 depict the models we found the most suitable, as far as the mission requirements are concerned.



Fig. 1: Bell Nexus 6HX. [3]



Fig. 2: Rolls-Royce EVTOL. [23]

The first prototype studied was the Bell Nexus 6HX (Fig. 1), a hybrid-electric Vertical Take-Off and Landing (VTOL), with a range of up to 241 kilometers and optimized for inter-urban mobility. The Nexus has six large ducted fans for vertical and forward flight, three on each side of the fuselage and a main high wing with a high rear stabilizer. [4]

Additionally, the Rolls-Royce EVTOL (Fig. 2) was the second concept taken into consideration. This hybrid-EVTOL configuration uses a gas turbine technology to generate electricity to power six electric propulsors, specially designed to have a low noise profile, allowing inner city operations. It also has a battery for energy storage. [24]



Fig. 3: Uber Elevate eCRM-001. [36]



Fig. 4: Archer Maker. [18]

Uber's eCRM-001 (Fig. 3) has four sets of stacked co-rotating propellers for vertical flight located on the tops of booms and on the fuselage and has one M-wing for forward flight. On top of that, its two propellers for forward flight can also tilt providing additional assistance for vertical take-off and landings. The aircraft is all electric, and, as Uber states, is the best solution for UAM and has been developed with a low environmental footprint in mind. [36]

The Archer Maker (Fig. 4) aircraft is focused on the improvement of mobility on dense markets with heavy traffic congestion, as well as in the increase of productivity of the aircraft through ride sharing. It has 12 electric propellers, six tilt-props for forward and VTOL flight, and six stationary propellers for VTOL-only flight. The aircraft is a sleek modern design with one main high wing, a V-tail and tricycle fixed wheeled landing gear. [18]

The Lilium Jet (Fig. 5) is an electric aircraft, composed by 36 electric engines, that allies high efficiency with a noise footprint low enough to be used in residential areas, since Lilium has developed a duct to absorb as much noise as possible from the electric motors. [14]

Lastly, Eve (Fig. 6) is an all electric aircraft with a human centered design, optimal safety, high

reliability, redundant systems, a lower noise footprint, to be community friendly, autonomous flight and no emissions. [11]



Fig. 5: Lilium Jet. [16]



Fig. 6: Eve. [11]

In addition, some relevant characteristics of these concepts are summed up in Tables 1 and 2.

	Bell Nexus 6HX	Rolls-Royce EVTOL	Uber Elevate eCRM-001
VTOL type	Tilt Duct	Tilted Wing	M-Wing
Propulsion	Hybrid-Electric	Hybrid-Electric	Electric
Capacity [Pax]	1 + 4 plus baggage	1 + 4/5	1 + 4
MTOW [kg]	2720	-	-
Cruise Speed [km/h]	287	402	241
Range [km]	241	805	96
Altitude [m]	-	-	1524

Tab. 1: Characteristics of some concepts already developed.

	Archer Maker	Lilium Jet	Eve
VTOL type	Tilt Propellers+V-Tail	Ducted Fan+Tilted Wing	Ducted Propellers
Propulsion	Electric	Electric	Electric
Capacity [Pax]	1 + 2 plus baggage	1 + 4/5/6 plus baggage	1 + 4 plus baggage
MTOW [kg]	3175	3175	-
Cruise Speed [km/h]	241	300	241
Range [km]	96	200-250	96
Altitude [m]	610	3000	800-1000

Tab. 2: Characteristics of some concepts already developed.

4 Aircraft Configuration and Conceptual Design

4.1 Concept Design

After gathering information on what the market already offers as a solution for our mission profile and design requirements, the group started focusing on the generation of a new concept in order to fulfill most of the mission requirements.

After a brainstorm of some concepts, and different drawing iterations, some solutions stood out as feasible and the group ended up with 6 different concepts that are going to be explained in the next subsections in greater detail.

4.1.1 Concept Design 1

This design has six Tilt-rotors with ducted fans, a footprint of 12x12 meters, a range superior to 100km with a cruise speed of 150km/h. The horizontal stabilizer is located above the wing. The capacity corresponds to 1 pilot + 4 passengers + luggage. The gross weight of this concept is of around 3000kg and it functions with hybrid-electric motors, with easy reconfiguration to all-electric.

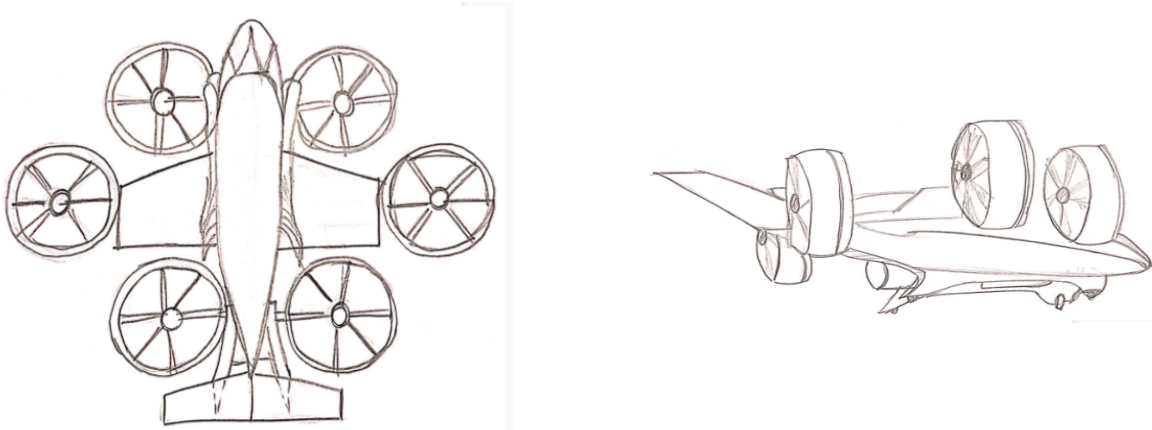


Fig. 7: Concept design 1

4.1.2 Concept Design 2

This design has six motors, four tilt-rotors and 2 with ducted fans. With a measurement of 15m length per 13m width, the model can fly for more than 100km at a cruise speed of 200km/h. Transporting a pilot and four passengers plus luggage, this concept weights around 2000kg and functions with hybrid-electric motors.

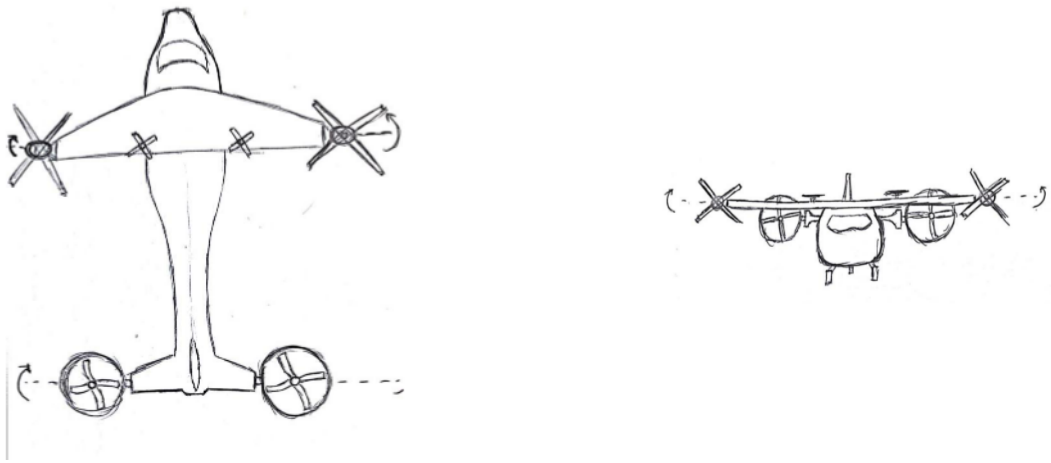


Fig. 8: Concept design 2

4.1.3 Concept Design 3

This concept has 12 motors (fans) with a footprint of 11m length per 10m width. It can fly for 150km at a cruise speed of 160km/h. Transporting a pilot and four passengers plus luggage, this concept weights around 2800kg and has electric propulsion.

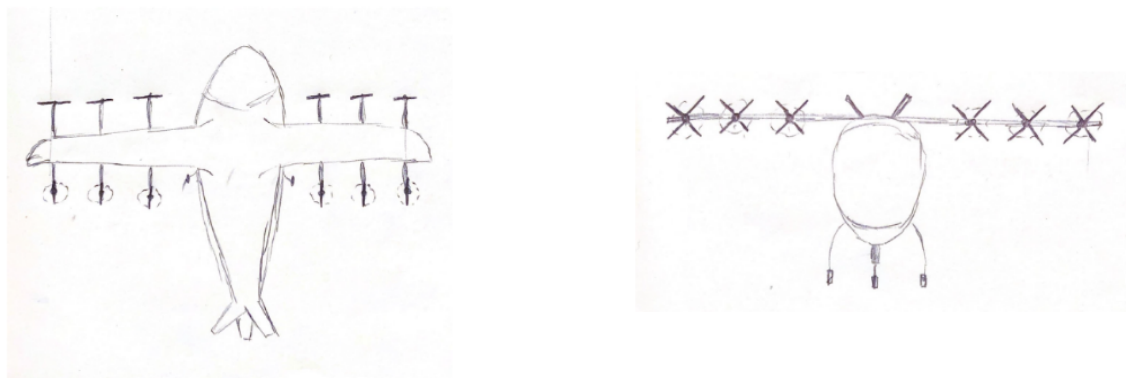


Fig. 9: Concept design 3

4.1.4 Concept Design 4

The fourth concept designed consists in a six motor configuration. With two tilt-rotors with ducted fans and two sets of stacked rotors, this configuration measures 8m in width and 10m in length. It has the capacity to fly 100km at a cruise speed of 120km/h, with fully electric motors. Transporting one pilot and two passengers plus luggage, its weight is of around 1500kg.



Fig. 10: Concept Design 4

4.1.5 Concept Design 5

In the fifth concept two tilt rotors are used. With a footprint of 13m length and 18m width, this concept is designed to fly over a distance of 250km at a cruise speed of 250km/h. It has capacity for a pilot and five passengers plus luggage weighting 3000kg. Motors are hybrid electric.

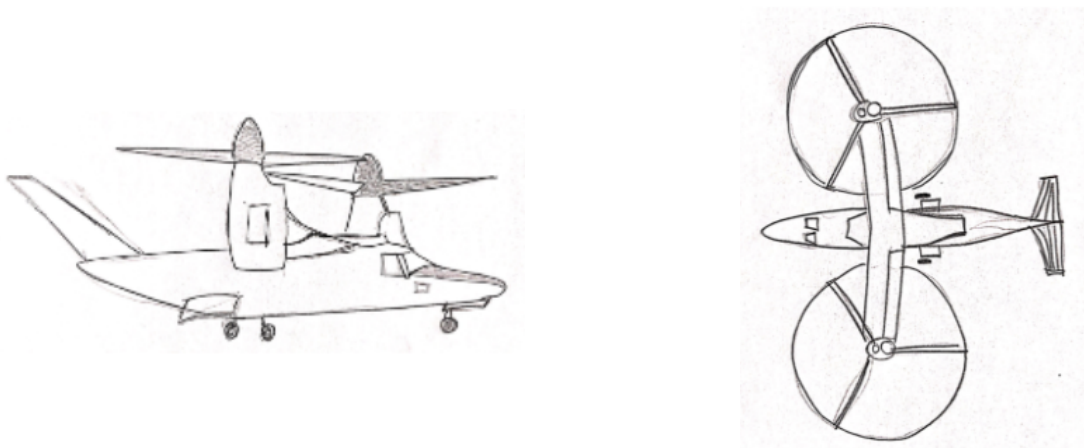


Fig. 11: Concept Design 5

4.1.6 Concept Design 6

This design has six motors, four in the tilted wing and two ducted fans. With a measurement of 12m length per 15m width the model can fly for 300km at a cruise speed of 300km/h. Transporting a pilot and six passengers plus luggage, this concept weights 3500kg and functions with hybrid electric motors.

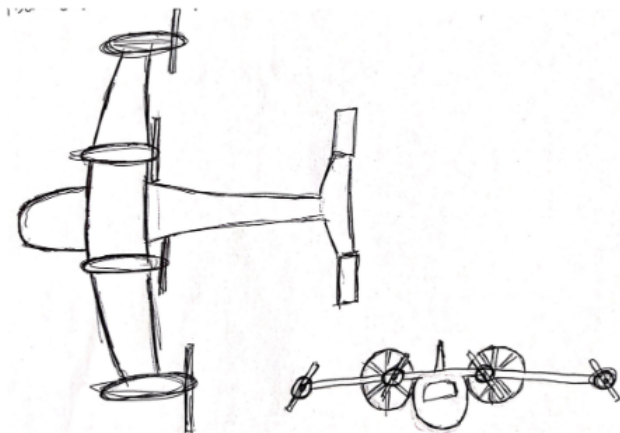


Fig. 12: Concept Design 6

4.2 Concept Choice

In order to select between the six different concepts developed earlier, we used a selection method, the analytical hierarchy process, to aid us. This method consists in defining the parameters that we think are the most relevant to the design, and attributing comparative values between these. By organizing these values in a matrix, the eigenvalues are computed and a comparative value between concepts is obtained. The criteria defined is presented in Figure 13.

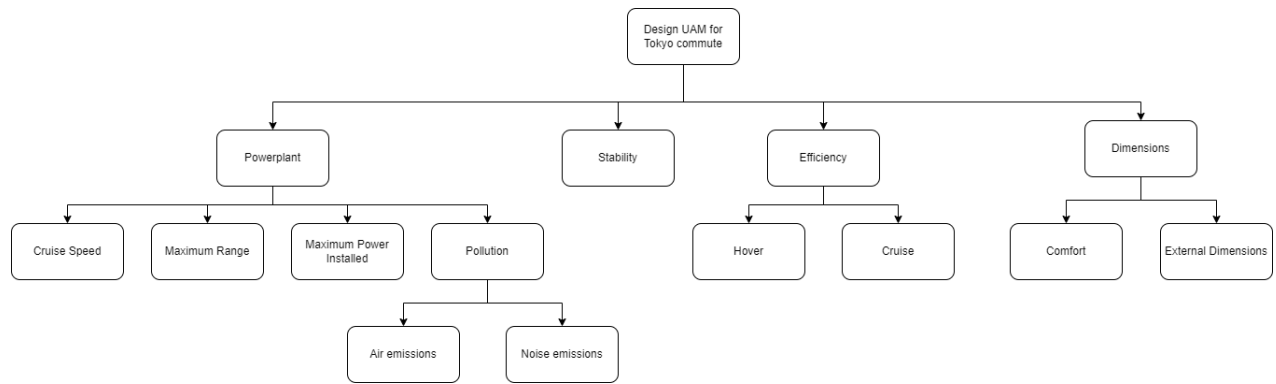


Fig. 13: Criterion Diagram

To compare the concepts developed, a scale of 1, of equal importance, to 9, of extreme importance, was used. These scores are relative, and must be interpreted from the line to the column, corresponding to an entry. As an example, in Table 3, the entry corresponding to the second line and first column is interpreted as "the stability criteria is more important than the powerplant criteria, with a score of 7". Using this grading scale, the comparative value between the same criteria is always 1, of equal importance. The score of two criteria in inverse order is always the inverse of the score attributed in the opposite order. In the case of the powerplant criteria and the stability criteria, the entry corresponding to line 1 and column 2 tells us that "the powerplant criteria is more important than the stability criteria, with a score of 0,14", which corresponds to 1/7 approximated to 2 decimal places.

Firstly the relative importance between the four main criteria was established. These scores are presented in Table 3

Criterion/Criterion	Powerplant	Stability	Efficiency	Dimensions
Powerplant	1,00	0,14	6,00	3,00
Stability	7,00	1,00	8,00	9,00
Efficiency	0,167	0,13	1,00	4,00
Dimensions	0,33	0,11	0,25	1,00

Tab. 3: Relative main criterion punctuation.

4.2.1 Powerplant

The powerplant used to power our aircraft is of the uttermost importance. The speed it must achieve, its maximum range before recharging or refuelling, the maximum power installed, and the pollution from its work are the criteria we defined as the most important, related to the powerplant. The pollution subcriteria is subdivided into two subcriteria, air emissions and noise emissions. The main subcriteria (cruise speed, maximum range, maximum power installed and pollution) are all relatively scored, and these scores are presented in Table 4. The scores attributed to each of the aircraft concepts in each of the subcriteria are presented in Table 5 for the cruise speed, Table 6 for the maximum range, and Table 7 for maximum power installed. Finally, the two subcriteria scores for pollution are presented. The two pollution subcriteria relative scores, air emissions and noise emissions, are presented in Tables 8 and 9. The mean values of the subcriteria is calculated, with equal pondering, in order to obtain a total value for the powerplant criteria. The mean values for the pollution subcriteria is presented in Table 10. The mean values for the powerplant main criteria is presented in Table 11

Subcriterion/Subcriterion	Cruise Speed	Maximum Range	Max. Power Installed	Pollution
Cruise Speed	1,00	6,00	5,00	0,13
Maximum Range	0,17	1,00	0,33	0,13
Max. Power Installed	0,20	3,00	1,00	0,13
Pollution	8,00	8,00	8,00	1,00

Tab. 4: Powerplant subcriteria relative scores.

Cruise Speed						
Concept/Concept	Concept 1	Concept 2	Concept 3	Concept 4	Concept 5	Concept 6
Concept 1	1,00	0,25	0,33	2,00	0,20	0,17
Concept 2	4,00	1,00	2,00	4,00	0,33	0,25
Concept 3	3,00	0,50	1,00	2,00	0,25	0,20
Concept 4	0,50	0,25	0,50	1,00	0,14	0,13
Concept 5	5,00	3,00	4,00	7,00	1,00	0,50
Concept 6	6,00	4,00	5,00	8,00	2,00	1,00

Tab. 5: Cruise speed relative scores.

Maximum Range						
Concept/Concept	Concept 1	Concept 2	Concept 3	Concept 4	Concept 5	Concept 6
Concept 1	1,00	1,00	0,33	2,00	0,20	0,17
Concept 2	1,00	1,00	0,33	2,00	0,20	0,17
Concept 3	3,00	3,00	1,00	4,00	0,33	0,25
Concept 4	0,50	0,50	0,25	1,00	0,14	0,13
Concept 5	5,00	5,00	3,00	7,00	1,00	0,50
Concept 6	6,00	6,00	4,00	8,00	2,00	1,00

Tab. 6: Maximum range relative scores.

Maximum Power Installed						
Concept/Concept	Concept 1	Concept 2	Concept 3	Concept 4	Concept 5	Concept 6
Concept 1	1,00	0,50	0,50	4,00	0,25	0,20
Concept 2	2,00	1,00	0,25	2,00	0,20	0,17
Concept 3	2,00	4,00	1,00	5,00	0,33	0,25
Concept 4	0,25	0,50	0,20	1,00	0,14	0,13
Concept 5	4,00	5,00	3,00	7,00	1,00	0,50
Concept 6	5,00	6,00	4,00	8,00	2,00	1,00

Tab. 7: Maximum power installed relative scores.

Air Emissions						
Concept/Concept	Concept 1	Concept 2	Concept 3	Concept 4	Concept 5	Concept 6
Concept 1	1,00	0,20	2,00	0,17	4,00	5,00
Concept 2	5,00	1,00	6,00	0,50	7,00	8,00
Concept 3	0,50	0,17	1,00	0,17	3,00	4,00
Concept 4	6,00	2,00	6,00	1,00	8,00	9,00
Concept 5	0,25	0,14	0,33	0,13	1,00	2,00
Concept 6	0,20	0,13	0,25	0,11	0,50	1,00

Tab. 8: Air emissions relative scores.

Noise Emissions						
Concept/Concept	Concept 1	Concept 2	Concept 3	Concept 4	Concept 5	Concept 6
Concept 1	1,00	0,17	0,33	0,13	0,50	1,00
Concept 2	6,00	1,00	3,00	0,50	4,00	4,00
Concept 3	3,00	0,33	1,00	0,20	2,00	2,00
Concept 4	8,00	2,00	5,00	1,00	6,00	7,00
Concept 5	2,00	0,25	0,50	0,17	1,00	1,00
Concept 6	1,00	0,25	0,50	0,14	1,00	1,00

Tab. 9: Noise emissions relative scores

Pollution						
Concept/Concept	Concept 1	Concept 2	Concept 3	Concept 4	Concept 5	Concept 6
Concept 1	1,00	0,18	0,57	0,14	0,89	1,67
Concept 2	5,50	1,00	4,00	0,50	5,09	5,33
Concept 3	1,75	0,25	1,00	0,18	2,40	2,67
Concept 4	7,00	2,00	5,50	1,00	6,86	7,88
Concept 5	1,13	0,20	0,42	0,15	1,00	1,33
Concept 6	0,60	0,19	0,38	0,13	0,75	1,00

Tab. 10: Pollution subcriteria mean scores

Powerplant						
Concept/Concept	Concept 1	Concept 2	Concept 3	Concept 4	Concept 5	Concept 6
Concept 1	1,00	0,32	0,41	0,48	0,26	0,23
Concept 2	3,13	1,00	0,52	1,23	0,30	0,25
Concept 3	2,44	1,94	1,00	0,62	0,38	0,30
Concept 4	2,06	0,81	1,61	1,00	0,19	0,17
Concept 5	3,78	3,30	2,60	5,29	1,00	0,59
Concept 6	4,40	4,05	3,34	6,03	1,69	1,00

Tab. 11: Powerplant subcriteria mean scores.

4.2.2 Stability

The relative scores for the stability criteria are presented in the Table 12. Since our mission profile concerns passengers transport, the vehicle stability is of great importance, which justifies the relative

score, attributed in Table 3.

Stability						
Concept/Concept	Concept 1	Concept 2	Concept 3	Concept 4	Concept 5	Concept 6
Concept 1	1,00	4,00	7,00	8,00	5,00	2,00
Concept 2	0,25	1,00	4,00	6,00	2,00	0,33
Concept 3	0,14	0,25	1,00	2,00	0,33	0,14
Concept 4	0,13	0,17	0,50	1,00	0,25	0,14
Concept 5	0,20	0,50	3,00	4,00	1,00	0,25
Concept 6	0,50	3,00	7,00	7,00	4,00	1,00

Tab. 12: Stability relative scores

4.2.3 Efficiency

Efficiency is also an important criterion for our mission. The transport of passengers between multiple points in the surroundings of a big city involves multiple take offs and multiple landings, which mean increasing energy spending. A good efficiency will allow our aircraft to perform more missions with no need to recharge electric batteries or top up fuel between flights. The relative importance of the efficiency subcriteria, efficiency in hover and efficiency in cruise, are presented in Table 13. The relative scores of both these subcriteria are presented in Tables 16 and 15. The mean values of both subcriteria on this criteria is presented in the table 14.

Subcriterion/Subcriterion	Hover	Cruise
Hover	1,00	0,13
Cruise	8,00	1,00

Tab. 13: Efficiency Subcriteria relative scores

Efficiency						
Concept/Concept	Concept 1	Concept 2	Concept 3	Concept 4	Concept 5	Concept 6
Concept 1	1,00	2,00	3,00	5,83	0,64	0,89
Concept 2	0,50	1,00	2,00	4,00	0,39	0,60
Concept 3	0,33	0,50	1,00	0,86	0,28	0,44
Concept 4	0,17	0,25	1,17	1,00	0,24	0,25
Concept 5	1,56	2,57	3,6	4,25	1,00	0,57
Concept 6	1,13	1,70	2,25	4,00	1,75	1,00

Tab. 14: Efficiency mean scores

Hover						
Concept/Concept	Concept 1	Concept 2	Concept 3	Concept 4	Concept 5	Concept 6
Concept 1	1,00	2,00	3,00	7,00	8,00	4,00
Concept 2	0,50	1,00	2,00	6,00	7,00	3,00
Concept 3	0,33	0,50	1,00	3,00	5,00	2,00
Concept 4	0,14	0,17	0,33	1,00	2,00	0,50
Concept 5	0,13	0,14	0,20	0,50	1,00	0,33
Concept 6	0,25	0,33	0,50	2,00	3,00	1,00

Tab. 15: Efficiency in hover relative scores.

Cruise						
Concept/Concept	Concept 1	Concept 2	Concept 3	Concept 4	Concept 5	Concept 6
Concept 1	1,00	2,00	3,00	5,00	0,33	0,50
Concept 2	0,50	1,00	2,00	3,00	0,20	0,33
Concept 3	0,33	0,50	1,00	0,50	0,14	0,25
Concept 4	0,20	0,33	2,00	1,00	0,13	0,17
Concept 5	3,00	5,00	7,00	8,00	1,00	2,00
Concept 6	2,00	3,00	4,00	6,00	0,50	1,00

Tab. 16: Efficiency in cruise relative scores.

4.2.4 Dimensions

The last main criterion defined was aircraft dimensions. An aircraft designed for urban air mobility must couple comfort with overall size. This mission profile is unfeasible for a plane with great dimensions, like those of a commercial airplane, but it must not be so small that the passengers are not having an enjoyable flight. The relative importance of the dimensions subcriteria, comfort and external dimensions, are presented in Table 17. The relative scores of both these subcriteria are presented in Tables 18 and 19. The mean values of both subcriteria in this criteria are presented in the Table 20.

Subcriterion/Subcriterion	Comfort	External Dimensions
Comfort	1,00	0,17
External Dimensions	6,00	1,00

Tab. 17: Dimensions subcriteria relative scores.

Comfort						
Concept/Concept	Concept 1	Concept 2	Concept 3	Concept 4	Concept 5	Concept 6
Concept 1	1,00	2,00	4,00	0,50	3,00	6,00
Concept 2	0,50	1,00	3,00	0,33	2,00	4,00
Concept 3	0,25	0,33	1,00	0,20	0,50	2,00
Concept 4	2,00	3,00	5,00	1,00	4,00	6,00
Concept 5	0,33	0,50	2,00	0,25	1,00	3,00
Concept 6	0,17	0,25	0,50	0,17	0,33	1,00

Tab. 18: Comfort relative scores.

External Dimensions						
Concept/Concept	Concept 1	Concept 2	Concept 3	Concept 4	Concept 5	Concept 6
Concept 1	1,00	0,20	0,14	0,13	0,33	0,50
Concept 2	5,00	1,00	0,50	0,33	2,00	4,00
Concept 3	7,00	2,00	1,00	0,50	4,00	8,00
Concept 4	8,00	3,00	2,00	1,00	6,00	8,00
Concept 5	3,00	0,50	0,25	0,17	1,00	3,00
Concept 6	2,00	0,25	0,13	0,13	0,33	1,00

Tab. 19: External dimensions relative scores.

Dimensions						
Concept/Concept	Concept 1	Concept 2	Concept 3	Concept 4	Concept 5	Concept 6
Concept 1	1,00	0,36	0,28	0,20	0,60	0,92
Concept 2	2,75	1,00	0,86	0,33	2,00	4,00
Concept 3	3,63	1,17	1,00	0,29	0,89	3,20
Concept 4	5,00	3,00	3,50	1,00	4,80	6,86
Concept 5	1,67	0,50	1,13	0,21	1,00	3,00
Concept 6	1,08	0,25	0,31	0,15	0,33	1,00

Tab. 20: Dimensions mean scores.

4.2.5 Concept Comparative Value

Finally, the matrices represented in the tables were input in a MATLAB program, which computed the eigenvalues of each and returned comparative values for each of our concepts. The closer a value is to 1 the better the model is. These values are presented in Table 21

Concept 1	0,3048
Concept 2	0,1555
Concept 3	0,0658
Concept 4	0,1064
Concept 5	0,1210
Concept 6	0,2465

Tab. 21: Analytical Hierarchy Process end results

Watching the results obtained, theoretically, the first concept is the best and is the one that we should choose. While developing the work related to the further section, we found some problems with the concept chosen, like the unnecessary number of rotors. For this reason, and a couple minor issues, we made some small modifications to the aircraft, reaching a final design. This final concept can be seen in figure 14. The big difference is the removal of the two rotors that were in the front of the first concept.

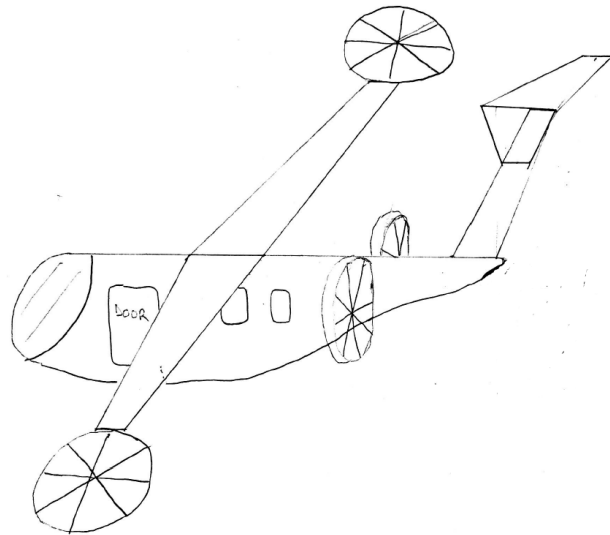


Fig. 14: Visualization of the final concept.

5 Aircraft Sizing and Design Point

As the aircraft concept and mission type have already been decided, the next step is to size the aircraft and determine its energy requirements. To do so, the mission profile has to be determined and, then, a mass estimation is performed based on historical data. These values are input on the Aircraft Design Tool. After this, the first iteration of the aircraft's development is complete. Nevertheless, some values obtained in this section will change throughout the work.

5.1 Mission Profile

In order to design the mission profile, the general requirements listed in section 3.2 had to be considered.

As it was previously mentioned in section 3.3.1, the typical mission is characterized by a moderate long cruise, so that the aircraft could perform, just like an "air taxi", the transportation of passengers between major cities in the country of Japan. The cities were chosen based on both its dimension and its distance from the capital. After the analysis, the result of the search is presented in table 22.

	Surrounding Cities	Distance [Km]
Tokyo	Tsukuba	53
	Utsunomiya	93
	Maebashi	101
	Matsumoto	165
	Nagano	170
	Iwaki	180
	Hamamatsu	183

Tab. 22: Chosen cities to implement the project and the distance between them and the capital of Japan.

Figure 15 depicts the map of this region, in which Tokyo is represented by a red circle and the nearby cities are marked with a red cross. As it can be observed, the distances differ from 50 up to

approximately 180 kilometers. As so, for the computation of the values in the MATLAB tool, we defined the range as a value of close to 150 kilometers. This radius is expressed in the figure by the dashed red circle.

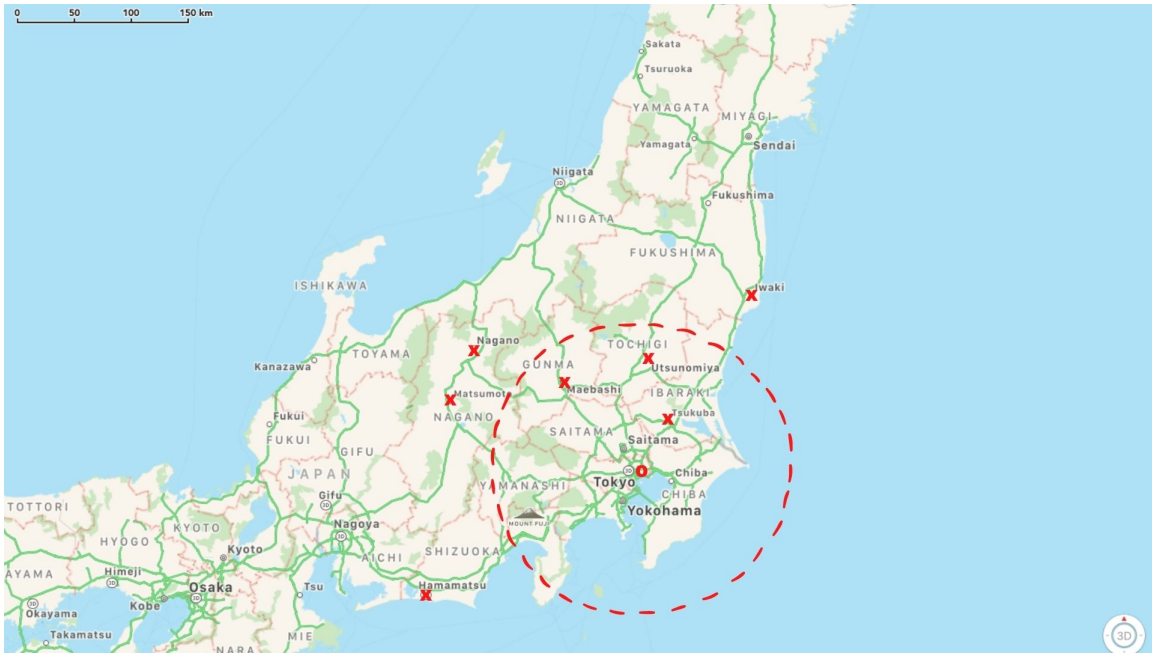


Fig. 15: Major cities in the city of Japan in which the service will be conducted.

Furthermore, there is the necessity to define each segment of this mission and the associated parameters. Such is resumed in table 23.

Segment	Initial Altitude [m]	Final Altitude [m]	Distance [m]	Speed [m/s]	Angle [°]	Segment Time [s]	Energy Source
Vertical Climb	0	150	0	4	-	37.5	Electric
Transition	150	150	1500	25	90	30	Electric
Climb	150	2500	10446.7	25	13	417.9	Fuel
Cruise	2500	2500	130000	59	-	2203.39	Fuel
Descent	2500	150	9079.7	-40	-15	227.0	Fuel
Vertical Descent	150	0	0	-4.0	-	37.5	Electric
Landing	0	0	0	-	-	30	Electric

Tab. 23: Mission segment's characterization.

Moreover, it is worth highlighting that the vertical climb has a maximum height of 2500m, which is what we found reasonable since higher heights imply more energy used. Besides, the speed does not surpass the limit of 4m/s in the vertical climb segment and the velocity of 59 m/s in cruise flight, so that the comfort of the passengers is assured.

With the help of the MATLAB tool, we can create the plot that can be seen in figure 16, which helps us better visualize our mission profile.

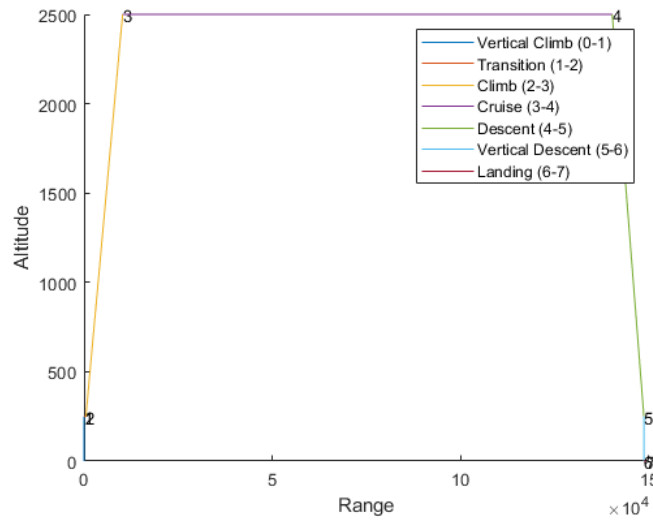


Fig. 16: Plot of our mission profile.

5.2 Maximum Take-off Weight Estimation - MTOW

Having established our mission profile, we can start the sizing process of our aircraft. We start by doing a mass estimation and computing the MTOW for our aircraft. The objective here is to find values for each component, based on mass fractions and the MTOW. For the MTOW computation, equation (1) will be used.

$$W_{T0} = \frac{W_{payload}}{1 - (MF_{Struct} + MF_{Subs} + MF_{Prop} + MF_{Energy})} \quad (1)$$

Taking into account our mission profile, we will make some estimates for the various mass fraction in equation (1), arriving to an estimate of the MTOW. Finally, with mass fractions and the MTOW, we can compute the various components masses.

For the payload weight, we will consider the weight of the crew, passengers and baggage. Since our aircraft will accommodate 1 crew member plus 4 passengers, we will consider a payload weight of $W_{payload} = 500\text{kg}$. Knowing that, through historical trends, $MF_{Struct} = 0.24$, and using the following formula

$$MF_{Subs} = \frac{3}{7}(MF_{Prop} + 0.24), \quad (2)$$

for the MTOW estimation, we just need to estimate MF_{Prop} and MF_{Energy} . Starting by MF_{Energy} , this mass fraction is divided into the batteries and the fuel, and by conducting some calculations for our mission segments, we arrive to a value of $MF_{Energy} = 0.3412$. For the mass fraction of the propulsive system, we need to take into account the electric and combustion motors, and the rotors. That being said, with some research into these masses for similar aircrafts, we got a value of $MF_{Prop} = 0.0804$. Using equation (2), the subsystems mass fraction ended up with a value of 0.1373.

We now have everything to compute W_{T0} , leading to a value of 2486.3kg. Having computed the value for the MTOW, we can use our mass fraction's estimates to find the masses for the various components of our aircraft. Obviously, the values that we will obtain are just a first estimate and throughout our work, these values will constantly change.

As we are trying to find the masses for all the aircraft's components, we first need to know in which group each component is (*Structures*, *Subsystems*, *Propulsion* or *Energy*). We already established that

the *Energy* group is divided into the batteries and the fuel. For the *Propulsion* group, we have the electric and combustion motors, and the rotors. Finally, for the *Subsystems* group we assumed that it consisted only of avionics components and the *Structure* group consisted of the fuselage and all the wings.

This distribution of mass between the components was in general easy to do, only the *Structure* group presented some additional difficulty. To help we used historical data. Therefore, we used the percentages that can be seen in figure 17 to compute the masses for all the wings and the fuselage.

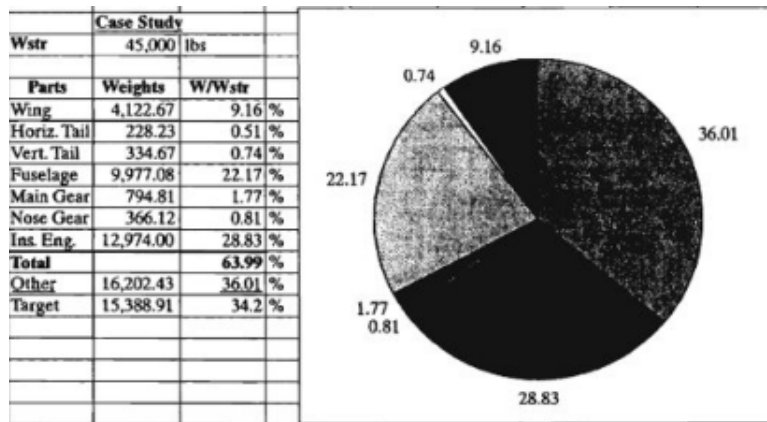


Fig. 17: Mass distribution for an aircraft. [12]

The mass values for all the components can be seen in table 24.

Component	Mass [kg]	Component	Mass [kg]	Component	Mass [kg]	Component	Mass [kg]
Crew	80	Fuselage	396	Turboshaft	129	Electric Motors	28
Passengers	320	Main Wing	180	Battery	360	Transmission	167
Avionics	343	Horizontal Tail	13.5	Fuel Tank	250	Gearbox	60
Payload Bay	100	Vertical Tail	9	Rotors	5	Generator	45

Tab. 24: Mass distribution throughout the components of our aircraft.

5.3 Design Point for Fixed Wing and VTOL

After the choice of the mission profile, it is necessary to determine the constraints of each of the mission's phases to determine the design point . After this, and using the aircraft design tools given, a plot of the design space and consequently of the design point, will be done.

5.3.1 Forward Flight Design Constraints

Range

Considering the range of a propeller aircraft, the optimal wing loading is given by the equation Eq.(3).

$$\frac{W}{S} = \frac{\rho V^2}{2} \sqrt{\frac{C_{D_0}}{k}} \quad (3)$$

where

$$k = \frac{1}{\pi A Re} \quad (4)$$

As the wing loading is independent of the power loading, this constrain will be a horizontal line in the $\left(\frac{W}{P}\right) - \left(\frac{W}{S}\right)$ plot. As the wing loading is the optimal one to maximize range, the design point should be located within the line, however the actual constrain is that the design point has to be located below this same line.

Cruise Speed

The power loading necessary to fly at cruise speed for a certain wing loading is given by the equation (5)

$$\frac{P}{W} \geq \frac{1}{\eta_p} \left[\frac{\rho V^3 C_{D_0}}{2(W/S)} + \frac{2k}{\rho V} \left(\frac{W}{S} \right) \right] \quad (5)$$

It is important to notice that the factor P/W reduces with the increase of W/S, which means that an increase in the area requires more power, as expected.

Climb Angle

Regarding the climb phase, the power loading for a given climb angle and wing loading is expressed in the equation (6)

$$\frac{P}{W} \geq \frac{V}{\eta_p} * \left[\sin \gamma + \frac{\rho V^2 C_{D_0}}{2(W/S)} + \frac{2k}{\rho V^2} \left(\frac{W}{S} \right) \right] \quad (6)$$

where γ is the climb angle and V, the climb velocity, is given by:

$$V = \sqrt{\frac{2}{\rho} \left(\frac{W}{S} \right) \sqrt{\frac{k}{C_{D_0}}}} \quad (7)$$

5.3.2 Vertical Flight Design Constraints

Vertical Climb

For the vertical climb, the constrain is described in equation (8)

$$\frac{W}{P} \leq \frac{1}{V_y - \frac{k_i V_y}{2} + \frac{k_i}{2} \sqrt{V_y^2 + 2 \frac{(W/A)}{\rho}} + \rho V_{tip}^3 \sigma \frac{C_d}{8(W/A)}} \quad (8)$$

This condition must be evaluated for both $\rho = \rho_0$ (density for the departure altitude) and $\rho = \rho_c$ (density for the ceiling altitude) and the constrain applied will be the most restrictive. The σ term represents the rotors solidity ratio.

Transition

The transition constraint combines the effects of the horizontal and the vertical flight condition. Here again a minimal power loading is needed to be able to full fill this flight manoeuvre.

$$\frac{W}{P} \leq \left(\frac{k_i}{\sin(\theta_{tilt})} \sqrt{\frac{-V_\infty^2}{2} + \sqrt{\left(\frac{V_\infty^2}{2} \right)^2 + \left(\frac{(W/A)}{2\rho \sin(\theta_{tilt})} \right)^2}} + \frac{\rho V_{tip}^3}{(W/A)} \left(\frac{\sigma C_d}{8} (1 + 4.6\mu^2) \right) + X \right)^{-1} \quad (9)$$

Where $X = \frac{1}{2} \rho V_\infty^3 C_{D_0} \frac{1}{(W/S)} + \frac{2(W/S)}{(\pi e R) \rho V_\infty}$.

5.3.3 Design Point

Since we have the components masses, and we also have defined the flight constraints, due to our mission profile characteristics, we now need to modify each component's characteristics in order to place our design point within the feasible range.

The main characteristics that were altered were the propulsive systems power, the main wing's area, by changing the aspect ratio and mean chord, and the rotors characteristics. These modifications were done taking into account what is present in the market right now, and it was a back-and-forth process until we stabilised a design point with which we were happy about it. As it was previously said, our goal was to place the points inside the working area, but always placing them the furthest from the origin possible.

By using the given aircraft design tool we end up with a final design point in figure 18.

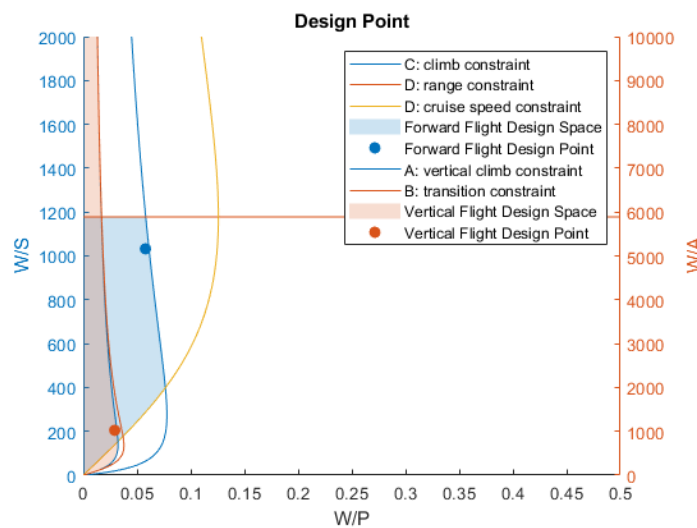


Fig. 18: Parametric analysis of the payload energy specific density and cruise speed

Further analysing these plot, we can determine our design point, specified below:

Design point forward flight

Wing Loading: 1032.25 N/m^2

Power Loading: 5.785 kg/kW

Design point vertical flight

Disk Loading: 1023.1 kg/m^2

Power Loading: 2.922 kg/kW

For the maximum take off weight, the MATLAB tool gave us a value of 2358.9kg, which was what we expected.

6 Wing Design

6.1 Wing Main Dimensions

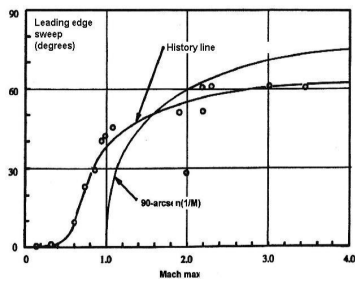
The Main Wing shape and dimensions will significantly affect the lift and drag produced and, consequently, the aircraft efficiency, one of the main targets in this task.

To illustrate the wing's development process until we reached the final design point shown in the previous section, based on the initial Maximum Take-Off Mass and the initial optimal wing loading obtained through the Design Point in the beginning of the design process, the total area was calculated, in order to better understand the other parameters that would be changed throughout the design.

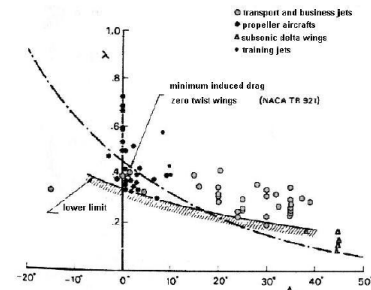
$$MTOM = 2621,5 \text{ Kg} \quad \frac{W}{S} = 1051,99 \text{ N/m}^2$$

$$S_{ideal} = 24,9 \text{ m}^2$$

In order to advance with the design, an initial Aspect Ratio of 7 was chosen. By constraining this value, initial results for span and mean chord were obtained. Furthermore, historical data was used to define the sweep angle and the taper ratio for the wings.



(a) Wing Sweep Angle chosen for different velocities.



(b) Taper Ratio chosen for different aircrafts.

Fig. 19: Historical trends for Wing Design.[28]

Given that the aircraft will cruise at speeds lower than Mach 0.3, the compressibility effects do not have any implications in the wing design, resulting in a sweep angle of zero, as per figure 19a. Given this sweep angle, according to figure 19b, the taper ratio to be used is 0.4. This will ensure that the wing's design is more efficient by reducing the amount of induced drag produced. [28]

After defining the initial values for the main wing design, an iterative process to obtain the most optimized design was done by improving the Design Point. In the end, the values for the final design were the following:

$$R = 6,55 \quad \bar{c} = 1,85 \text{ m} \quad b = 12,1 \text{ m} \quad S = 22,4 \text{ m}^2$$

6.2 Airfoil Selection

The process of choosing the airfoil for the main wing of the aircraft is extremely important because it will affect the pressure distribution around the wing, which will impact the lift and drag forces produced by the wing. Therefore, it is necessary to obtain the more optimized airfoil possible.

Before starting the selection of the airfoil it is mandatory to understand the conditions where we are operating in. For that we calculated the Reynolds number, Re for the mean chord of the wing. The calculation was done using the equation 10, considering the air properties for the cruise altitude and the cruise velocity.

$$Re = \frac{\rho V c}{\mu} \quad (10)$$

For the cruise altitude of 2500m and for the cruise velocity of 56m/s, $Re = 6.2 \times 10^6$.

Based on literature, it was decided that a good option to explore was the 4 digits NACA airfoils family, where the first digit gives the maximum camber, the second one the position of maximum camber and the last two the thickness/chord ratio. Firstly, we select the NACA XX12 and NACA XX14 airfoils, because the $(t/c)_{max}$ of the aircraft is expected to be in between these values according to literature (for Mach = 0.163 for cruise speed). So, the airfoils NACA 2412, NACA 2414, NACA 4412, NACA 4414, NACA 6412 and NACA 6414 were studied and compared with more detail.

The curves of C_l vs α , C_d vs α , C_m vs α , C_l vs C_d and C_l/C_d vs α , obtained with the software XFLR5, for the six airfoils for the Reynolds number calculated with the mean chord of the wing can be seen in the figure 20. Looking at the results, the 64xx airfoils were discarded because, although they present better results for the lift coefficient C_l , the moment coefficient C_m was much higher in absolute value than the others. This moment will need to be compensated by other surfaces, like the tail, that will need to increase in area, which is not wanted. Now, considering that according to literature the $(t/c)_{max}$ of the aircraft is expected to be a little lower than 14%, it was decided to explore only the airfoils NACA XX12. In the table 25 it's possible to see a more precise comparison between these two airfoils. [27]

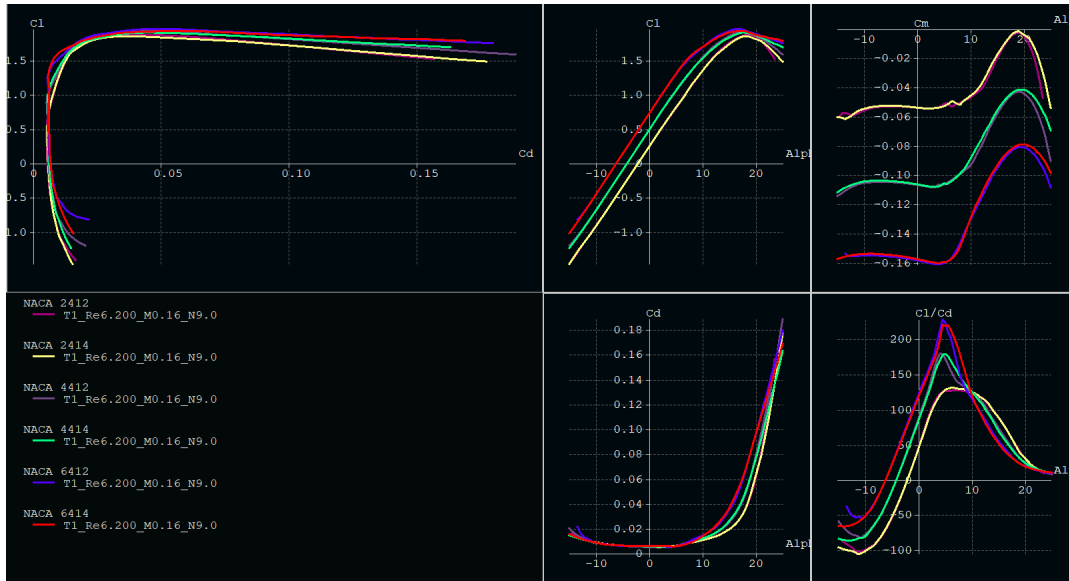


Fig. 20: Comparison of the 6 NACA airfoils

Looking at the table it is important to understand what to expect from the different parameters and how the comparison was done.

From the C_d vs α plot, the value for C_{dmin} is obtained, which is wanted to be the lowest possible, so that the wing produces less drag, leading to a need of smaller engines and, therefore, less weight; from the C_l/C_d vs α graph, the maximum value of C_l/C_d is obtained, wanted to be the highest possible; from the graph of C_m vs α , the value for C_{m0} (moment coefficient at the zero lift angle) was obtained, supposed to be close to zero, so that the other surfaces that have to compensate this moment, normally the tail, do not need to have higher areas than the necessary; from the C_l vs α graphic, values for $C_{l\alpha}$, C_{lmax} , α_0 (zero lift angle) and α_{stall} (stall angle) are taken. The stall angle represents the angle at which the aircraft will start losing the equilibrium and may fall, so, for safety reasons, this value is wanted to be as high as possible. The zero lift angle is the angle at which the aircraft has a lift of zero. It is

Tab. 25: Comparison of some properties for the NACA 2412 and NACA 4412 airfoils

	NACA2412	NACA4412
$C_{l\alpha} [/\text{rad}]$	6.42	6.42
$C_{l\max}$	1.87	1.92
$\alpha_0 [\text{°}]$	-2.15	-4.2
$\alpha_{stall} [\text{°}]$	19	18
$(Cl/Cd)_{\max}$	127	180
$C_{d\min}$	0.005	0.005
C_{m_0}	-0.053	-0.1

desired that this angle has a negative value, so that the lift is higher at a zero angle of attack and the comfort of the passengers is assured.

Taking in consideration all these aspects above, and trying to find the best compromise among all of them, we decided to choose the NACA 4412 airfoil. The airfoil's properties can be seen in the figure 21, for a range of Reynolds numbers that included the ones in the tip and root chord, in this way a complete analysis of the wing could be done.[27]

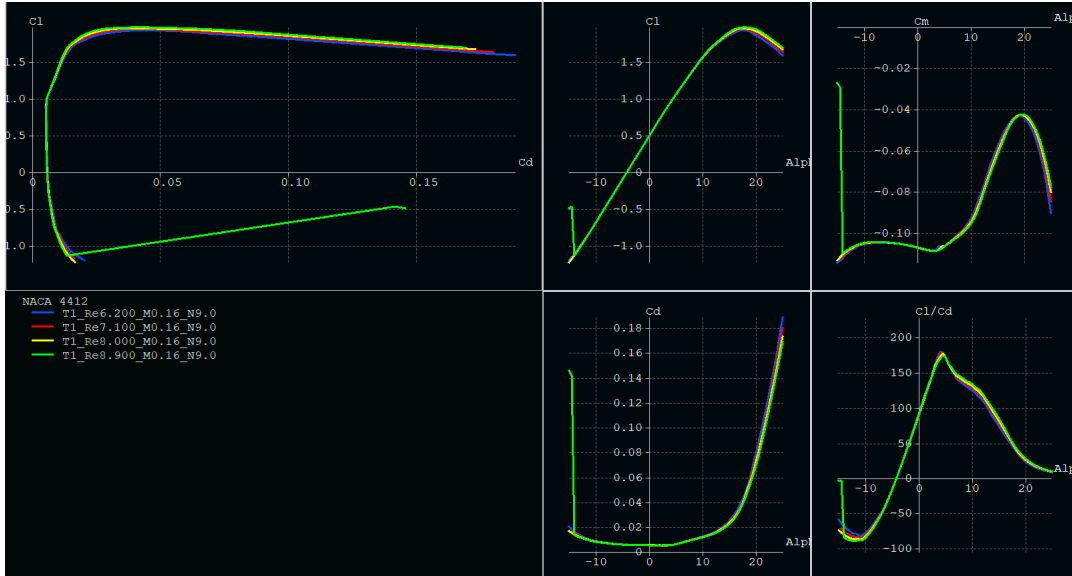


Fig. 21: NACA 4412

6.3 Lift and Drag Estimation

The wing designed is not infinitely large, which will cause the overall Coefficients of Lift and Drag to change from the predicted values given previously. Some factors such as the aspect ratio and the downwash will have direct implications on the final coefficient of lift obtained. The resultant lift slope can be calculated using the following formulae:

$$C_{L\alpha} = \frac{c_{l\alpha} \cdot AR}{2 + \sqrt{4 + (AR \cdot \beta)^2(1 + \frac{\tan^2(\Lambda_{t/c}\max)}{\beta^2})}} \quad (11)$$

$$\beta = \sqrt{1 - M_{\text{effective}}^2} \quad M_{\text{eff}} = M_\infty \cos(\Lambda_{LE})$$

$c_{l\alpha}$ is the airfoil derivative of lift coefficient with respect to the attack angle. After calculating the value of $C_{L\alpha}$, one can obtain the relation between the Lift slope and the resultant Lift using the equations in 12.

$$C_L = C_{L\alpha}\alpha + C_{L\alpha=0} \quad C_{L\alpha=0} = -\frac{dC_L}{d\alpha}\alpha_0 \quad (12)$$

After computing all of the variables, an equation for the resultant lift can be written:

$$C_L = 0,0814\alpha + 0,3417 \quad (13)$$

It is important to make sure that the angle used in equation 13 is in degrees. To perform the drag estimation, similar steps can be done. In this case, a prediction can be made based on the base Drag (C_{D_0}) and the Lift induced drag (kC_L^2), ignoring the effects of losses.

$$C_D = C_{D_0} + kC_L^2 = C_{D_0} + \frac{1}{\pi e R} C_L^2 \quad (14)$$

In equation 14, e represents the Oswald efficiency factor, assumed to be 0,85 in every aerodynamic component of the aircraft. Ideally, the real base Drag would be equal to the theoretical base Drag, but due to imperfections in the manufacturing processes and to the connection between the wing and the fuselage or the rotors, the real base Drag shall be higher than the theoretical value. This Drag can be calculated using equation 15, where C_f is the viscous drag coefficient (Eq. 17), F is the form factor (equation 18), Q is the interference factor, assumed to be 1,2 due to the rotors at the end of the wing, and S_{wet}/S is the relation between the wet area of the wing and the wing area, given by 19.

$$C_{D_0} = C_f F Q \frac{S_{wet}}{S} \quad (15)$$

$$Re_x = \frac{V \cos(\Lambda_{LE}) \bar{c}}{v} \quad (16)$$

$$C_f = \frac{0,455}{(\log_{10} Re_x)^{2,58} (1 + 0,144 M^2)^{0,65}} \quad (17)$$

$$F = \left[1 + \frac{0,6}{(x/c)_{(t/c)_{max}}} \left(\frac{t}{c} \right)_{max} + 100 \left(\frac{t}{c} \right)_{max}^4 \right] \times [1,34 M_{cr}^{0,18} (\cos(\Lambda_{[t/c]_{max}}))^{0,28}] \quad (18)$$

$$\frac{S_{wet}}{S} = 1,977 + 0,52(t/c)_{max} \quad (19)$$

Using the equations mentioned, each value can be computed and an equation for the drag obtained:

$$C_D = 0.00038\alpha^2 + 0.0032\alpha + 0.0089$$

6.4 Wing's Location

It was chosen to place the wing in a higher position due to stability improvements. So, the wing is a high wing, which means it is mounted on top of the fuselage.

7 Tail Design

7.1 Tail Sizing

The first consideration for the tail design was its shape and configuration. Based on the several options available, as seen in figure 22, the T-tail was deemed the best option for the aircraft. Although this solution might be heavier than the others, the efficiency of the vertical tail is increased due to the work of the horizontal tail as a winglet. Furthermore, the horizontal tail is less affected by the wake of the main wing and also the rotors placed rearwards in the fuselage.

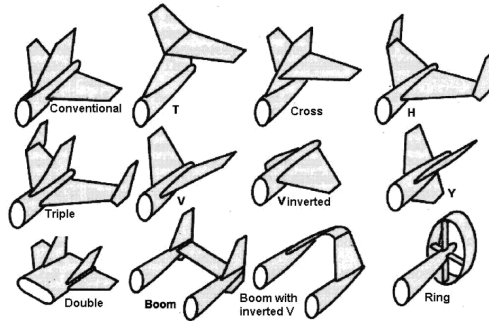


Fig. 22: Possible tail shapes and configurations.[26]

By analysing historical values, the initial volume coefficients for both horizontal and vertical tail were obtained from figure 23. The volumes used for the twin turboprop were the ideal to be used in the aircraft, with a 5% reduction in the horizontal volume due to the selection of the T-tail. In the end, the values used initially were $V_H = 0,85$ and $V_V = 0,08$.

	Typical Values	
	V_H	V_V
Glider	0,50	0,02
"Homebuilt"	0,50	0,04
General Aviation – Single Engine	0,70	0,04
General Aviation – Twin Engine	0,80	0,07
Agriculture aircraft	0,50	0,04
Twin turboprop	0,90	0,08
Hydroplane	0,70	0,06
Training jet	0,70	0,06
Fighter	0,40	0,07
Military transport/Bomber	1,00	0,08
Civilian transport	1,00	0,09

Fig. 23: Volume Coefficient historical values.[26]

The volume coefficients can be calculated through the following formulae:

$$V_H = \frac{S_H l_H}{S_W \bar{c}_W} \quad V_V = \frac{S_V l_V}{S_W b_W} \quad (20)$$

In the equations 20, l_H and l_V refer to the distance between the aerodynamic center of the Main Wing and the aerodynamic center of each tail. To predict other initial sizing values, historical data for taper and aspect ratio were analysed, resulting in early sizing values of $AR_H = 5$, $AR_V = 1,2$, $\lambda_H = 0,6$ and $\lambda_V = 1$.

	Horizontal Stabilizer		Vertical Stabilizer	
	A	λ	A	λ
Fighter	3.0 a 4.0	0.2 a 0.4	0.6 a 1.4	0.2 a 0.4
Glider	6.0 a 10.0	0.3 a 0.5	1.5 a 2.0	0.4 a 0.6
Other	3.0 a 5.0	0.3 a 0.6	1.3 a 2.0	0.3 a 0.6
T tail	-	-	0.7 a 1.2	0.6 a 1.0

Fig. 24: Historical values for taper and aspect ratio.[26]

Moreover, the leading edge sweep defined for the horizontal tail represented a small increment to the angle of sweep of the main wing. Given the low Mach number of the cruise speed of the aircraft, the sweep for the horizontal tail is only 5 degrees on the trailing edge. In addition, a trailing edge sweep angle of 35 degrees was chosen for the vertical tail, based on other aircraft values. [26]

After several iterations, the final sizing for the tail was obtained, ending with the following values:

$$AR_H = 5 \quad \bar{c}_H = 0,8 \text{ m} \quad \Lambda_{\text{Horizontal trailing edge}} = 5^\circ$$

$$AR_V = 2 \quad \bar{c}_V = 0,95 \text{ m} \quad \Lambda_{\text{Vertical trailing edge}} = 35^\circ$$

7.2 Airfoil Selection

The selection process for the vertical and horizontal tail airfoil is almost identical to the one described for the main wing. Firstly, the Reynolds number is calculated with the cruise conditions and with the respective mean chords. For the horizontal tail, $Re = 2.5 \times 10^6$, and for the vertical tail, $Re = 3 \times 10^6$.

From the information obtained in the literature, it was decided to explore the 4 digits NACA airfoils family (that we described previously), more specifically the airfoils NACA 0009 and NACA 0012. In the figures 25 and 26, the curves of C_l vs α , C_d vs α , C_m vs α , C_l vs C_d and C_l/C_d vs α , obtained with the XFLR5 software, can be visualized. The figure 25 and the figure 26, are respectively concerning the horizontal tail and the vertical tail, both for the two airfoils considering the Reynolds number calculated with the mean chord of each tail. [27]

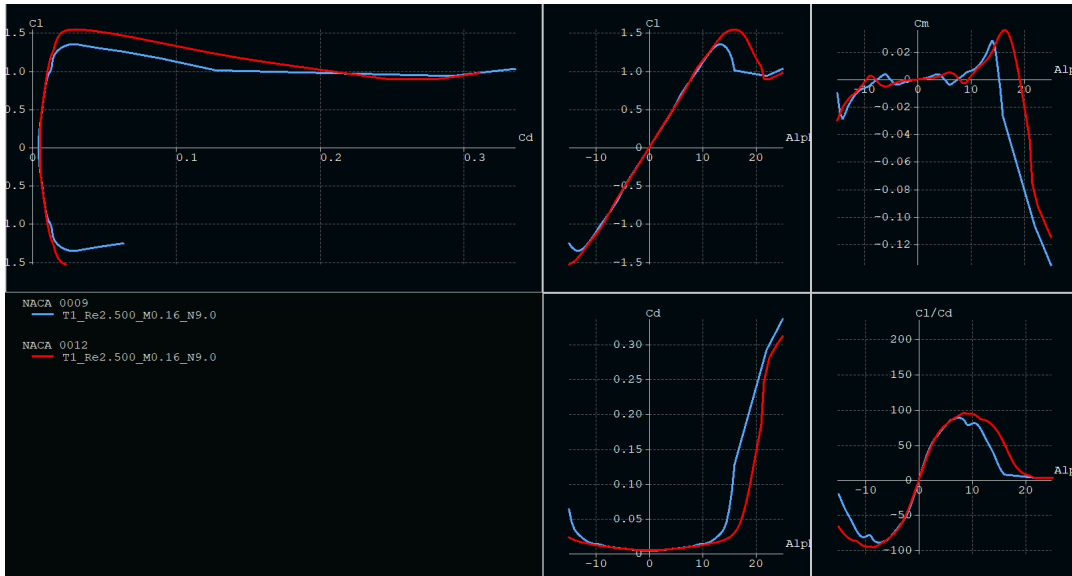


Fig. 25: Comparison of the NACA 0009 and NACA 0012 for the Horizontal Tail

In the Tables 27 and 28, the properties of both airfoils, for the vertical and horizontal tail, are summarised.

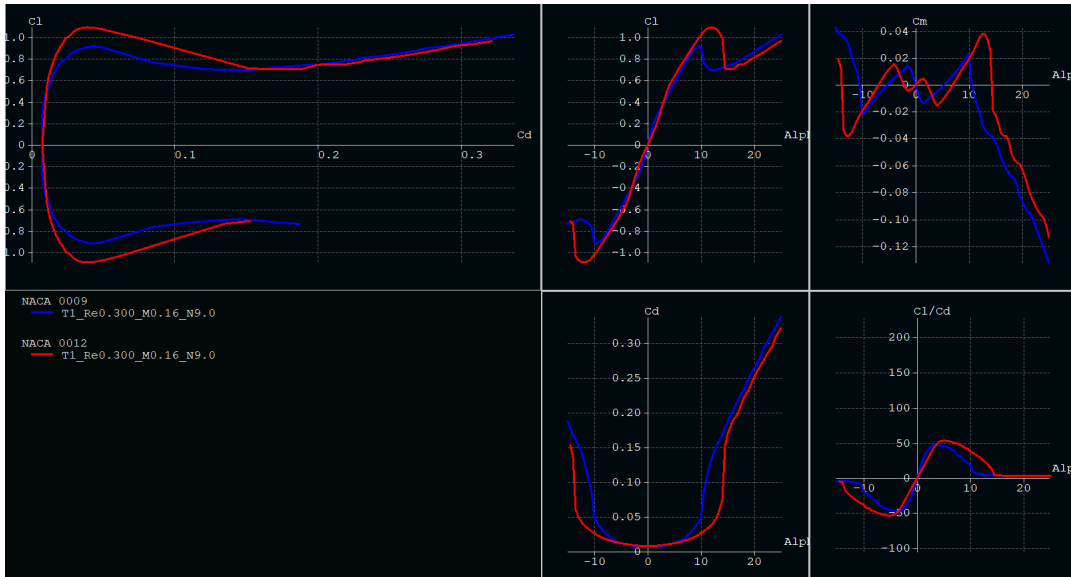


Fig. 26: Comparison of the NACA 0009 and NACA 0012 for the Vertical Tail

As said before, a lot of parameters should be taken into account to choose the airfoil: the value for the $C_{d_{min}}$, that is wanted to be the lowest possible; the maximum value of C_l/C_d , that is wanted to be the highest possible; the values of C_{l_α} , $C_{l_{max}}$, α_0 (zero lift angle, in this case is 0 for both airfoils because they are both symmetrical) and α_{stall} (stall angle), which values are wanted to be as high as possible. Notice that the value of C_{m_0} is 0 for both airfoils because they are both symmetrical. [27]

Taking all these aspects into account, the best compromise found corresponds to choosing the NACA 0012 for both the vertical and the horizontal tails.

Tab. 26: Tail

Tab. 27: Vertical tail

	NACA0009	NACA0012
$C_{l_\alpha} [rad]$	6.65	7.33
$C_{l_{max}}$	0.92	1.09
$\alpha_0 [^\circ]$	0	0
$\alpha_{stall} [^\circ]$	9	12
$(Cl/Cd)_{max}$	47	53
$C_{d_{min}}$	0.0074	0.0077
C_{m_0}	0	0

Tab. 28: Horizontal tail

	NACA0009	NACA0012
$C_{l_\alpha} [rad]$	6.47	6.55
$C_{l_{max}}$	1.35	1.54
$\alpha_0 [^\circ]$	0	0
$\alpha_{stall} [^\circ]$	13	16
$(Cl/Cd)_{max}$	89	95
$C_{d_{min}}$	0.0044	0.0051
C_{m_0}	0	0

7.3 Drag estimation

Due to the symmetry of the airfoil chosen, it won't produce lift, so $D = D_0$ and $C_D = D_{D_0}$. With this in mind, by applying equations 15 to 19, the formulae for the tails' drag coefficients can be obtained:

$$C_{D_{horizontal}} = 0.0021 \quad C_{D_{vertical}} = 0.0020$$

8 Propulsive System Design

In this section the entire process of propulsive system design is going to be addressed. This was a very dynamic system along the whole project, in the sense that some major modifications had to be made several times, as well as several studies to support those modifications. On that account, it is worth mentioning that although power plant studies were carried out after the first propulsion studies, we think that this subject should be addressed in the first place on this report.

8.1 Power Plant

Taking into account our mission profile and our requirements, the first decision made by the group was to feature a hybrid propulsive system implemented in such a way that the power delivered to the rotors could be purely electric. Simultaneously, an ICE would run a generator which, in turn, would recharge the batteries. Besides not being able to find supporting bibliography for this principle, we acknowledged that the *JSON* file was not prepared for this kind of architecture. As such, we had to come up with another solution, in which the VTOL phases are carried out using fully electric propulsion, and the remaining phases of the flight are carried out using only fuel propulsion (traits of a parallel propulsive system design). The main reason for opting this is that fully electric propulsive systems produce less noise than fuel ones. Furthermore, since current energy density in batteries is somehow low, and the VTOL phases are quite expensive in terms of power, a fuel alternative was chosen for the rest of the flight. Nevertheless, during the non VTOL flight phases, the ICE is not only powering the rotors, but also a generator that allows some battery recharge.[29]

The main difficulty when designing the power plant was to think of a simple connection between each energy source and the rotors that would allow an easy switch between sources. The solution found was to feature a transmission following the ICE (and, in the first iteration, the electric motors), with a clutch that engages the selected power source and disengages the one that is not being used. However, after realizing that four coaxial rotors was a better solution than four simple rotors (this will be addressed in detail in the next section), the electric motors were placed right next to the rotors, instead of being put inside the fuselage, near the transmission. This means that only the ICE is connected to the transmission, and that there must be a clutch for each two rotors.

The first and last iterations of the power plant can be observed in figure 27.

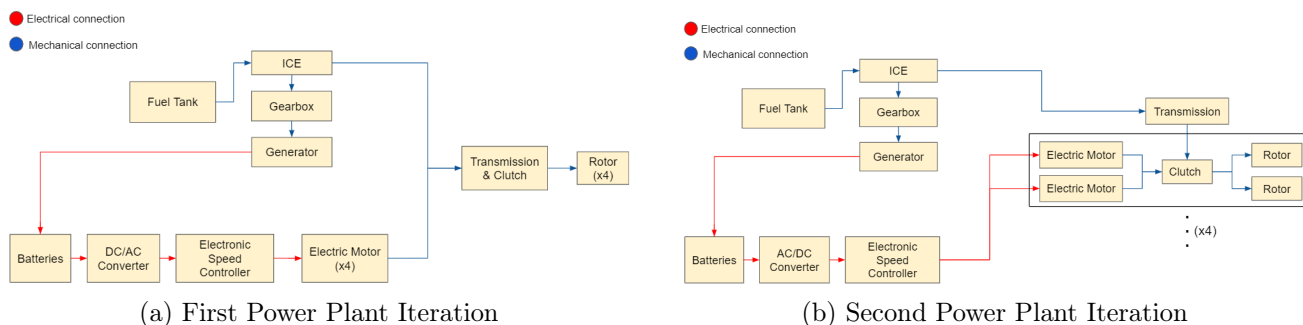


Fig. 27: Power Plant Evolution

8.2 Rotors

The rotors are a fundamental part as far as the propulsive system is concerned. Thus, the number of rotors implemented, the power requirements, its dimensions and specifications have to be studied in detail.

Firstly, the group decided it would be best to use four rotors in a duct fan configuration (since it is more efficient than an open propeller), with five blades each, in order to allow a more distributed weight loading, and reduction in vibratory loads (which handles a smoother flight). Along with the number of blades, the first chosen parameters were the radius, R of the blade, and solidity of the rotor, σ . Initially, the solidity of the rotor, was adjusted based on the output of the *JSON* file, by always trying to place the design point at an optimum location. Furthermore, knowing that the solidity of the rotor is given by

$$\sigma = \frac{Nc}{\pi R} \quad (21)$$

where N is the number of blades, the ratio $\frac{c}{R}$ was defined as 0.1 (since this is a pretty common order of magnitude), and a first guess of 0.13m was made for the chord, which handled a radius of 1.3m.[15]

In a more advanced stage of the project, a more thorough study was made on the propulsive system, which output a better approximation for the radius of the rotor's blades. Standing on the principle that all rotors are equally sized, we started with the equation

$$N_{\text{rotors}}\pi R^2 = \frac{mg}{(W/A)} \quad (22)$$

where N_{rotors} is the number of rotors, m is the *MTOW* of the aircraft, g is the gravitic acceleration, and W/A is the disk loading (note that both the *MTOW* and the disk loading are outputs of the *JSON* file), which handled $R = 1.3416m$. The solidity of the rotor was maintained, since the initial value has proven to give the best design point results.[30]

Nevertheless, as the total dimension of the aircraft was almost surpassing the usual length of the helipads, the group concluded that the originally considered rotors could be replaced by some other rotors that fitted best this requirement. Furthermore, as the main advantage of the contrarotating rotor design is that the net size of the rotors is reduced, for a given aircraft gross weight, the group concluded that coaxial rotors could be implemented.[15]

Hence, a study on the variation of the rotor radius with the number of rotors per axis was conducted. It is important to highlight that it was admitted that all of the rotors needed to output the same power and the area of each rotor was proportionally inverse to the number of rotors. The results are summarized in Table 29.

N_{rotors} / axis	Rotor Area [m²]	Rotor Radius [m]
1	5.64	1.34
2	2.655	0.92

Tab. 29: Rotor Area and Radius for single and coaxial rotors

The radius of the rotors markedly decreases when the number of rotors per axis increases, arguing in favour of the group's choice. Nonetheless, another factors needed to be taken into account, such as the extra power that would, consequently, need to be installed to the same area. In fact, the two coupling rotors interact with one another, producing a more complicated flow field than a single rotor, incurring a loss of net rotor system aerodynamic efficiency. In addition, one can not assume that the output power of the pair of coaxial rotors is the same as the sum of the total power provided by each one. As so, an estimation of the power that had to be installed was conducted for both mission segments VTOL and cruise, so that they could provide the sufficient thrust. Such results are presented in Table 30.[15]

This estimation was computed following the equation $P_{\text{installed}} = \sqrt{2}P_{\text{needed}}$, which takes into account the interference-induced power factor. $P_{\text{installed}}$ is the power that has to be provided to the rotors by

	$P_{\text{needed}} \text{ (2 Isolate Rotors) [W]}$	$P_{\text{installed}} \text{ (Coaxial Rotor) [W]}$
VTOL	24664.8	34881.3
Cruise	5130.8	7256.1

Tab. 30: Power needed per Rotor for single and coaxial rotors

the motors (corrected) and P_{needed} is the power that was previously computed in the design point.[15]

In the first iterations, the group thought about only replacing the front rotors. Nevertheless, that would imply that the control system would be much more difficult to implement, since different values of power would have to be delivered to different pairs of coaxial rotors. As so, this idea was rejected. Having this in mind, four coaxial rotors were implemented, two in the front and two in the back.

Moreover, in order to have an overview of the total power, some other estimations were made which are presented in Table 31.

	VTOL	Cruise
Total power without coaxial rotors [W]	98659.2	20523.2
Total power with coaxial rotors [W]	139525.2	29024.4

Tab. 31: Total power for single and coaxial rotors

As it can be observed, the extra power that had to be given is not very high. Thus, this conjecture will be the one used for the aircraft.

8.3 Minimum Power Required

Before choosing any kind of motor, it is important to have an idea of the minimum power that we need, so that a lower boundary can be established. As such, some calculations were performed, in order to obtain the value of such boundary.

8.3.1 VTOL

As the calculations should be performed for the worst case scenarios, the maximum hover altitude (150m) was considered, since the power requested to the motors will assume its highest value (during VTOL phases, the whole weight of the aircraft has to be compensated by the lift generated by the rotors, and air density is minimum at maximum altitude).

The first step was to determine the thrust required per rotor, T_r . Since in hover, the generated thrust, T , must be equal to the weight, W , we can write [30]

$$T_r = \frac{W}{N_{\text{rotors}}} \quad (23)$$

Having calculated the thrust required per rotor, we can use equation (22) to calculate the radius of the blades, and use that value to calculate the maximum rotation speed of the rotor, n_{\max}

$$v_{\text{tip,max}}^2 = (n_{\max} \pi D)^2 \Leftrightarrow n_{\max} = \frac{v_{\text{tip,max}}}{\pi D} \quad (24)$$

where $v_{\text{tip,max}}$ is the maximum velocity at the tip of the rotor, and D is the diameter of the rotor.[30]

Finally, with the rotational speed defined, we can estimate the power that produces the required thrust. This is an iterative process that starts with a guess for the needed power, P , after which the power coefficient, C_P , is computed

$$C_P = \frac{P}{\rho n_{\max}^3 D^5} \quad (25)$$

where ρ is the air density at the hovering altitude.[30]

After computing the value of C_P , we need to get the value of the ratio $\frac{C_T}{C_P}$ (being C_T the thrust coefficient), which can be done by analysing the plot shown in figure 28.[30]

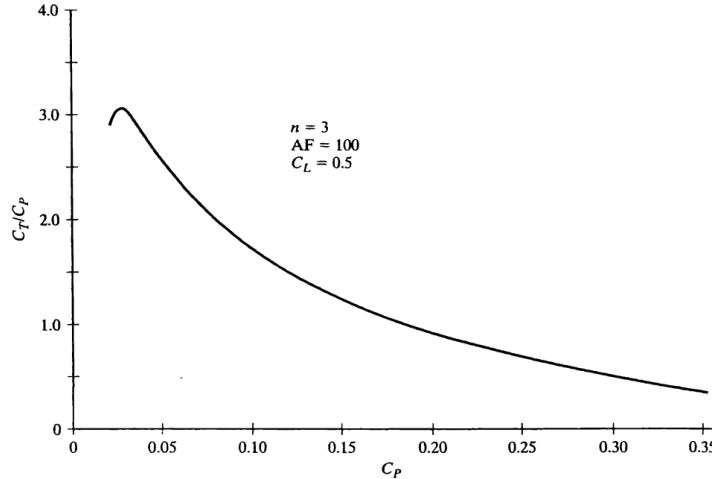


Fig. 28: $\frac{C_T}{C_P}$ as a function of C_P (three-blade propeller, $C_L = 0.5$, AF=100) [6]

After obtaining a value for the ratio $\frac{C_T}{C_P}$, the thrust can be calculated using

$$T = \frac{P}{n_{\max} D} \frac{C_T}{C_P} \quad (26)$$

Nevertheless, since the plot is related to a three-blade propeller, a correction for the thrust generated must be applied. Following the trend shown in figure 29, we decided to apply a correction factor of 1.1 for the thrust generated, since our rotor has five blades.[30]

Performance	2 blades	3 blades	4 blades
Efficiency	$1.03\eta_p$	η_p	$0.97\eta_p$
Thrust	$0.95T$	T	$1.05T$

Fig. 29: Thrust and efficiency correction factor for different numbers of rotor blades [6]

Lastly, having determined the corrected thrust, T^* , we just have to compare it with the value obtained from equation (23), and evaluate whether it is enough or not. In case it is not enough or far greater, a new guess for the power should be made (the goal is to get a value of T^* as close as possible from T_r).[30]

As an output from this method, we got a minimum power required for VTOL of 145kW/rotor for the simple rotor concept, and 75kW/rotor for the coaxial rotor concept.

8.3.2 Cruise Flight

In order to check whether the calculated minimum required power for cruise flight is enough or not, we need to start by calculating the minimum required thrust. This can be done by starting with a cruise drag estimation. As such, we start by calculating the cruise drag coefficient, $C_{D_{cr}}$, resorting to the drag polar

$$C_{D_{cr}} = C_{D_0} + \frac{1}{\pi AR e} C_{L_{cr}}^2 \quad (27)$$

in which C_{D_0} is the base drag coefficient (output of the *JSON* file), AR is the aspect ratio of the main wing, e is the Oswald efficiency factor (assumed as 0.8), and $C_{L_{cr}}$ is the lift coefficient in cruise. Since in cruise flight, the lift must be equal to the weight of the aircraft, $C_{L_{cr}}$ can be determined using

$$C_{L_{cr}} = \frac{mg}{\frac{1}{2} \rho v_{cr}^2 S} \quad (28)$$

in which v_{cr} is the cruise velocity, and S is the main wing reference area (output of the *JSON* file).[30]

Having a value for $C_{D_{cr}}$, we can now use the drag formula to calculate the total drag of the aircraft in cruise flight [30]

$$D_{cr} = \frac{1}{2} \rho v_{cr}^2 S C_{D_{cr}} \quad (29)$$

As in cruise flight the thrust must be equal to the drag, we are able to determine the thrust required per each rotor [30]

$$T_r = \frac{D_{cr}}{N_{rotors}} \quad (30)$$

Again, we want to maximize the rotor's performance, so we maximize the rotational speed of the rotor. As such, the maximum rotational speed can be computed using [30]

$$v_{tip,max}^2 = v_{cr}^2 + (\pi n_{max} D)^2 \Leftrightarrow n_{max} = \frac{\sqrt{v_{tip,max}^2 - v_{cr}^2}}{\pi D} \quad (31)$$

For cruise flight, we can estimate C_P based on the advance ratio, J , which is given by the ratio of the true air speed to the tip speed of the rotor [30]

$$J = \frac{V_{cr}}{n_{max} D} \quad (32)$$

Having the rotor's advance ratio, we can get a value for C_P by analysing the plot shown in figure 30, and assuming an efficiency, η_P , (which should be the highest possible).[30]

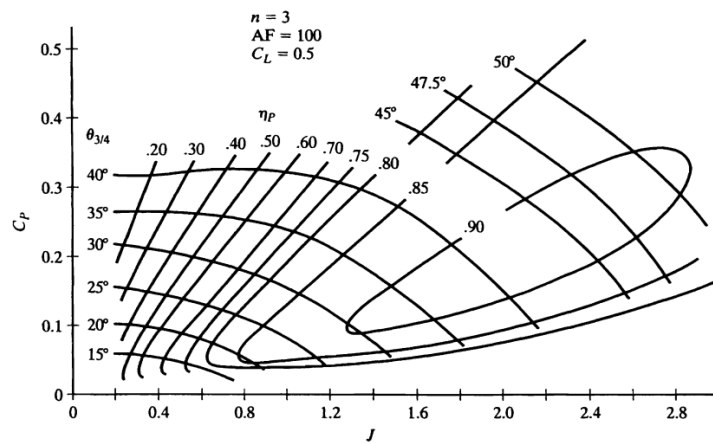


Fig. 30: C_P as a function of J , η_P , and blade pitch at 75% of its length, $\theta_{3/4}$ (three-blade propeller, $C_L = 0.5$, AF=100) [6]

It's important to note that for each value of J , and for a given efficiency, there are two possible values of C_P (one for a higher value of $\theta_{3/4}$, and another for a lower value of $\theta_{3/4}$). In order to minimize the required power, the lowest value of C_P should be chosen.[30]

Having obtained a value of C_P , we just need to solve equation (25) for P , in order to obtain the required power.[30]

Finally, we have to check whether it is possible or not to generate the thrust required per rotor with the obtained power. This can be done solving the following equation for T

$$P = \frac{T v_{cr}}{\eta_P} \quad (33)$$

When solving equation (33), it is important to remember that the value chosen for η_P must be corrected, since the plot in figure 30 assumes a three-blade propeller. The correction factor can be consulted in the table shown in figure 29. Once again, following the trend of the data in the table, we chose a value of 0.94 for the correction factor, since our rotors have five blades.[30]

As an output from this method, we got a minimum power required for cruise of 93kW/rotor for the simple rotor concept, and 46kW/rotor for the coaxial rotor concept.

Regarding what has been done in sections 8.3.1 and 8.3.2, we need to point out four essential aspects. Firstly, these calculations are not very accurate, for example, because of the difficulty in reading accurately the plots in figures 28 and 30, or the approximations taken while estimating the drag of the aircraft. Secondly, the required power is higher than the obtained values, since this method does not make a distinction between eight simple rotors and four coaxial rotors (the latter need more power when compared to the former, considering that the dimensions are the same). Thirdly, as said before, this results only establish a lower boundary for the required power for each flight phase. The chosen values for the installed power were obtained through a trial and error method, by trying to place the design point at an optimum location, using the *JSON* file. Lastly, it is important to mention that the $\sqrt{2}$ correction factor for coaxial rotor power was not applied here, since this study was used as a reference for the *JSON* file, which also doesn't make a distinction between eight isolate rotors and four coaxial rotors.

8.4 Components choice

Using the data obtained from the design point, the group made a market study on commercial components that could be used to build a propulsive system that features all the constraints and requirements.

8.4.1 Electric Motors

For the sake of simplicity, the group found that having an electric motor per rotor would be better. Furthermore, since any needed difference in generated thrust between the front and back rotors will be applied by the control system, all motors can be similar. As such, the design point dictated that the aircraft should feature eight electric motors with a maximum power of 100kW each. However, this power must be correct by a factor of $\sqrt{2}$, in order to account for the coaxial rotors. Hence, a power of 141kW is needed. It is important to mention that besides the mass of the motor, the fact of including or not a gearbox was also a crucial parameter, since this component can be quite heavy. The information obtained in the market study is summarized in Table 32.

If the four simple rotor configuration was kept, the *APM200* would be the chosen motor, since it includes a gearbox, and it was the one that has proven to place the design point at the best location. Nevertheless, since the final configuration was the four coaxial rotor one, the choice switched to the *APM120*. Even though the installed power value for the maximum power of each motor is slightly

Tab. 32: Electric motors and respective specifications [1][2][7][8][34]

Motor	P_{\max} [kW]	RPM	Mass [kg]	Efficiency	Gearbox
EMRAX228	109	6500	12.4	0.92-0.98	not included
APM120	120	12000	14	-	included
EMRAX268	200	4500	20	0.92-0.98	not included
APM200	220	10000	42	-	included
Siemens SP260D	261	2500	50	0.95	not needed

higher, the *APM120* is the one that has the closest value, while complying with the mass and gearbox constraints. Hence, this motor could be modified, in order to comply with all the requirements.

Fig. 31: *APM120* [8]

8.4.2 Internal Combustion Engine and Generator

The internal combustion engine is only connected to the rotors during forward flight. At first, the group was thinking about 4-stroke piston engines. However, after some research, we realized that the specific power of this type of engines is much lower than what we were aiming for. As such, we decided that a turboshaft engine would suit better our project. Once again, the installed power was dictated by the design point, and has a value of 390kW, which after corrected by a factor of $\sqrt{2}$ gives 552kW. The data we obtained in the market study is shown in Table 33.

Tab. 33: Turboshaft engines and respective specifications [5][9][10][22]

Engine	P_{\max} [kW]	Output shaft speed RPM	Mass [kg]
RR500TS	283	2358 or 2030	113
PT6B-9	373	6230	116
PW206A	410	6240	107.5
PW207D1	455	6240	110.9
LTS101-850B-2	556	6780	129.2

Again, if the four simple rotor configuration was kept, the *PW207D1* would be the chosen engine, since it was the one that has proven to place the design point at the best location. However, since the final configuration was the four coaxial rotor one, the choice switched to the *LTS101-850B-2*. As it happened with the electric motor, the *JSON* file output for the engine power was slightly higher. As such, the chosen turboshaft has to be tuned, in order to meet our requirements.



Fig. 32: *LTS101-850B-2* [17]

For the generator, the research was more unsuccessful in the sense that only one option was found. Its specifications can be consulted in Table 34

Tab. 34: Generator specifications [13]

Generator	P [kW]	Rotation speed RPM	Mass [kg]
Honeywell	200	18000 - 24000	45

Since it was the only option found, the *Honeywell* was the chosen one. Note that because of the higher rotation speed of the generator, when compared to the turboshaft's output shaft speed, a gearbox must be included in order to connect both components.



Fig. 33: *Honeywell generator* [13]

8.4.3 Transmission and Gearbox

Since there is only one ICE and there are four coaxial rotors, we needed to think of a way to distribute the generated power by the rotors. The solution found was quite similar to what is used in helicopters: a transmission. Unfortunately, the market study revealed itself to be completely unsuccessful when trying to find a commercial transmission. However, in order to be able to predict at least the mass of this component, we found a common weight-to-power ratio range of 0.18 – 0.30kg/kW. Since these components were the last ones to be included, a weight-to-power ratio of 0.3 was chosen, as this value was the one that placed the design point at the best location. Hence, we obtained a mass of 167.4kg for the transmission and 60kg for the gearbox.[20][37]

9 Fuselage Design

In this section we will define our fuselage. A fuselage has many different purposes depending on the type of mission. According to our mission, the tasks of the fuselage are accommodating the crew, passengers, baggage, cargo, and all the necessary equipment to a safe flight. It also has the structural purpose of supporting the wing, the stabilizers and landing gear.

We will follow a procedure to design the fuselage as explained in [31].

9.1 Volume Considerations

The first thing to do is to see space requirements for this kind of aircrafts and this type of mission. It's a short-range mission, carrying 4 passenger plus 1 crew, with a maximum of 100kg of baggage in total.

The fuselage cross-section is going to be defined according to recommended values for some of the components dimensions. In Table 35, we can see the recommended and chosen values.

	Recommend Values	Chosen Values
Seat Width [m]	0.41-0.46	0.5
Seat Pitch [m]	0.76-0.81	0.8
Aisle Height [m]	min. 1.52	1.778
Aisle Width [m]	min. 0.38	0.75

Tab. 35: Passengers compartment requirements and chosen values.

It was chosen a fuselage of 2 meters of diameter, which allowed us to have a fuselage compartment of 0.222m as it can be seen in figure 34

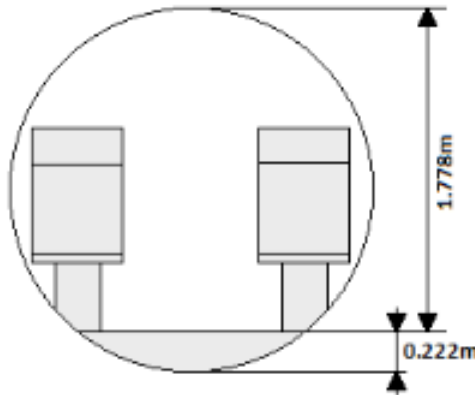


Fig. 34: Fuselage cross-section.

Before we move forward, it is important to note that the main wing will intersect the fuselage right on top of it, needing a wing carry-through structure. The size of this wing carry-through structure is equal to the thickness of the wing in its root, which has already been defined when we designed the main wing. Since the thickness of the wing is the largest at its root, this will help withstand the large bending moments on the wing.

9.2 Emergency Exits Requirements

We also need emergency exits for our passengers and crew to get out of the aircraft, safely. In fact, in a case of emergency, all passengers must be able to safely evacuate the aircraft in less than 90s. Because of it, FAR 25.807 demands at least a *Type IV* emergency exit, since we only have 4 passengers. The installation of this type of exit, requires it to be on top of the main wing, but since our aircraft has its wings on top of the fuselage, we'll choose a *Type II* exit. The door's dimensions are 0.508m in width, 1.118m in height and a corner radius of 0.169m. This type of door coincides with the floor level, as it can be seen in figure 35.

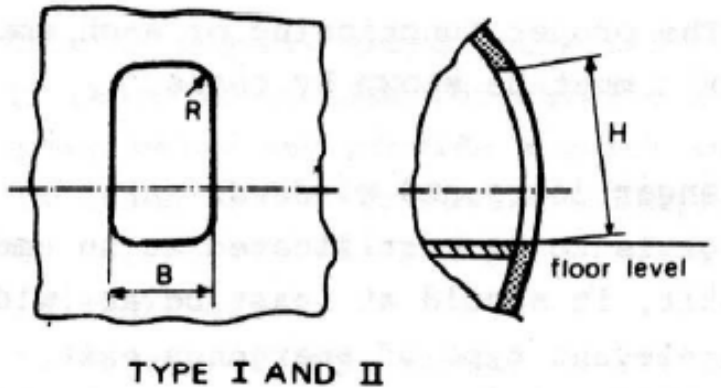


Fig. 35: Emergency exit required for passenger transport aircraft by FAR 25.807 for *Type II*.

Looking at the figure, we can associate the door's dimensions to each letter. This is shown in table 36

Parameter Value	
B [m]	0.508
H [m]	1.118
R [m]	0.169

Tab. 36: Dimensions for a *Type II* emergency exit door.

9.3 Landing Gear design

Since we can land our aircraft vertically, we can choose between two types of landing gear, skids or wheels. Both have advantages and disadvantages. If an aircraft has a landing gear with wheels, in case of a motor malfunction, the aircraft can do an emergency landing since the wheels would allow a horizontal landing. The skids don't have that ability, but they have the advantage of being lighter, producing less drag and not requiring complex retractable mechanisms and fuselage space.

Balancing all the advantages and disadvantages of both types of landing gears, it was chosen a skid landing gear for our aircraft. For its placement, we have to choose the point below the center of gravity of the aircraft, which will be defined in section 10. For its dimension, we used historical data for similar type of aircraft and ended up with the following skid. It is worth noting that the small hole in the landing gear is functional, since it works as a step for people to get on the vehicle.

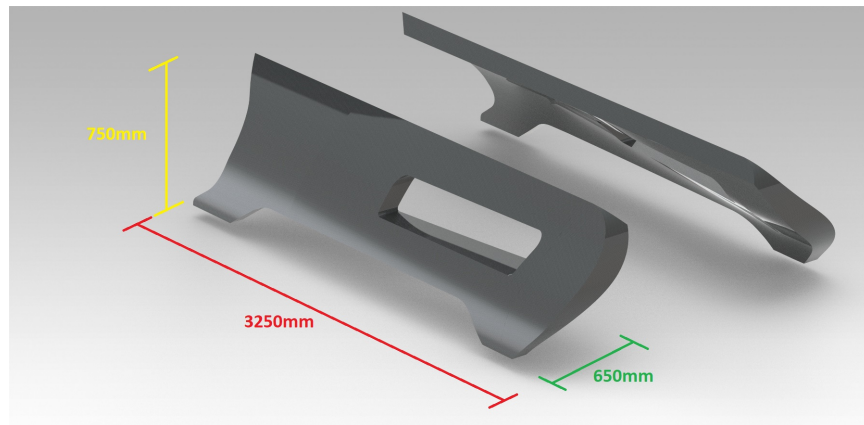
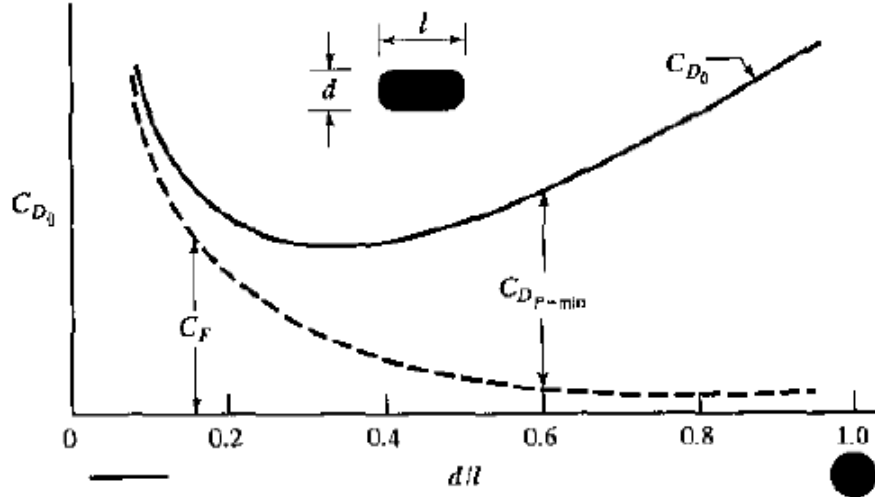


Fig. 36: CAD model of the landing skid

9.4 Aerodynamic Considerations

we still need to define the fuselage length, and for that we will take into consideration the fuselage fineness ratio, which is the ratio between the fuselage maximum diameter and its length. As previously seen before we defined our maximum diameter as 2 meters. Using this, we can see the following figure which gives us C_{D_0} as a function of the fineness ratio for subsonic flight, and can choose the ratio that minimises C_{D_0} .

Fig. 37: C_{D_0} as a function of the fuselage fineness ratio.

Looking for its minimum, we can see that it is around $\frac{d}{l} = 0.3$. As we are going to need some space to accommodate all the necessary components, it was chosen a fuselage fineness ratio of 0.25, instead of 0.3 as previously said. For these two values, the difference in C_{D_0} is minimal, so we aren't compromising the aircraft's aerodynamics. The value of $\frac{d}{l} = 0.25$, gives us a length for the fuselage of 8 meters.

9.4.1 Fuselage Shape

Now that the main geometric parameters are defined, we can draw a sketch of the fuselage. However, some important aerodynamic considerations need to be taken into account.

One of the many objectives for any aircraft, is to have the biggest lift to drag ratio. The fuselage will be the main source of drag in our aircraft. Furthermore, it's a component that doesn't produce much lift, so it's in our best interest that the fuselage has the best aerodynamic shape, given the length and maximum diameter already defined.

The best aerodynamic shape is the one that is the smoothest with the least gradual changes in curvature and without creating angles between surfaces. The purpose of this is to not separate the flow of air around the fuselage, which would lead to a major increase in drag. In figure 38 we can see the first sketch of our fuselage, showing its side and top view.

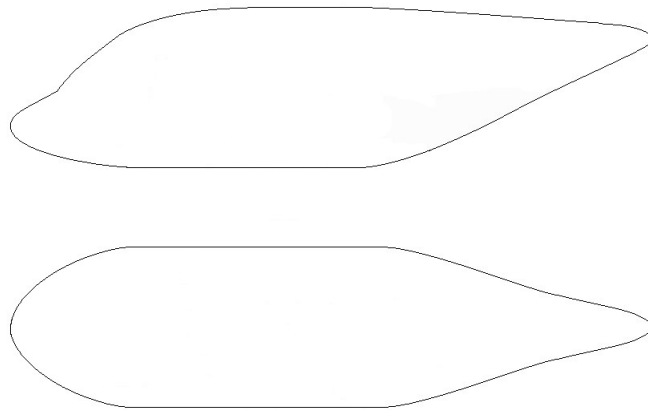


Fig. 38: Sketch of the fuselage shape. The first sketch is a side view and the second is a top view.

9.4.2 Drag Estimation

Now that we defined the fuselage, we should estimate its drag coefficient and some more important quantities. The drag coefficient can be written as

$$C_{D_0} = \frac{F_f + F_w}{\frac{1}{2}\rho V^2 S} \quad (34)$$

where ρ is the air density, V is the aircraft velocity, S is the wing area and F_w is the wave drag which we will neglect since our flow is subsonic. The term F_f can be expressed as

$$F_f = \frac{1}{2}\rho V^2 S_{wet} C_f \mathcal{F} Q \quad (35)$$

An estimation of the wetted area, $S_{wet} = 1.7(A_{top} + A_{side})$ leads to a value of 39.1m^2 . For the interference factor, \mathcal{F} , it depends on the fuselage fineness ratio, and is $\mathcal{F} = 2.0375$, the form factor, Q , it was estimated to be ≈ 1.2 to account for some rotor and wings interference. For the friction drag coefficient, C_f , since it depends on the reynolds number, we first need to calculate it, $Re_x = 25149768.4$, which will give a value of $C_f = 0.0025943$.

We can now calculate $F_f = 413.1\text{N}$ and estimate the drag coefficient, $C_{D_0} = 0.01106$.

10 Weight Distribution

In this section, we will allocate the various components of our aircraft, across the fuselage and wing. This work will be very important since it will influence the static stability analysis and in turn, will determine if our concept is feasible or not. Our goal here, is to distribute the various components so that the longitudinal position of the center of gravity of the aircraft is in front of its aerodynamic center.

In Table 37, we can see a table where we put the longitudinal position of each component and its masses. In this table we can also see where the center of gravity will end up, as well as the static margin.

	Mass [kg]	Position x [m]
Fuselage (CG)	396	2.4
Main Wing (root leading edge - CG)	180	2.68 - 3.37
Horizontal Tail (root leading edge - CG)	13.5	8.05 - 8.45
Vertical Tail (root leading edge - CG)	9	6.8 - 7.2
Turboshaft (CG)	129.2	6.2
Battery (CG)	360	1.2
Fuel Tank (CG)	250	3.2
Transmission (CG)	167.4	4.96
Gearbox (CG)	60	5.46
Coaxial Rotors 1/2 (CG)	10+10	2.68
Coaxial Rotors 3/4 (CG)	10+10	6.57
Electric Motor 1/2 and 3/4 (CG)	28+28	2.68
Electric Motor 5/6 and 7/8 (CG)	28+28	6.57
Crew (CG)	80	1.6
Passengers (CG)	320	3.4
Avionics (CG)	343	0.64
Payload Bay (CG)	100	4.32
Generator (CG)	45	5.77
Skids (CG)	96	2.978
Aircraft (CG)	2701.1	2.978
Static Margin	8.89%	-

Tab. 37: Longitudinal center of gravity position of each components. The distances are measured from the front of the nose of the fuselage.

Note that the fuselage length is 8 meters. The positions shown in figure 37 can be seen in a more appealing manner in figure 39.

Note that the electric motors are not present in figure 39, since they are alongside the coaxial rotors on the tip of the main wing.

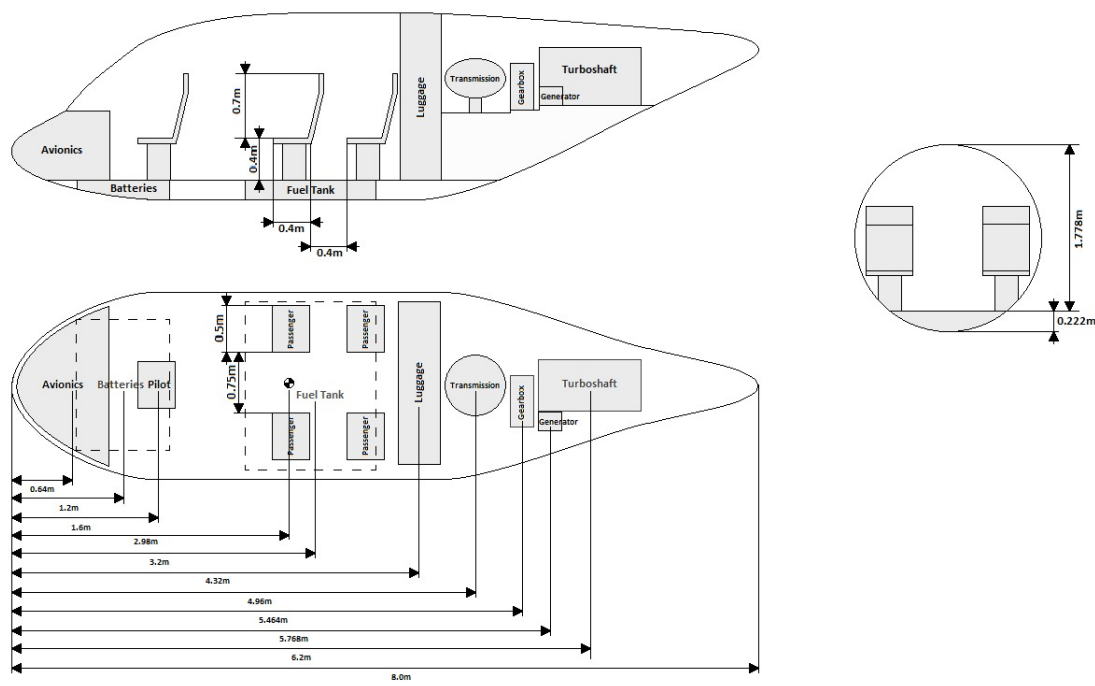


Fig. 39: Graphic visualization of the fuselage interior, showing the components distribution.

11 Static Stability

An aircraft is said to be stable if it tends to return to an equilibrium position after some perturbation, under steady flight conditions. It is always desired to have a stable aircraft, since it is more safe and requires less input from the pilot. The more an aircraft is stable, the less manoeuvrable it becomes, and having an aircraft that is too hard to maneuver is a problem. Therefore, the static stability analysis is a trade-off between these two concepts.

We will study the longitudinal, lateral and directional stability of our aircraft. In the following analysis, a conventional aircraft will be assumed, which does not vary much from our aircraft.

11.1 Longitudinal Stability

This type of stability, focus on the pitching motion of the aircraft. For this analysis, we need the derivative of the pitching moment coefficient with respect to the angle of attack, C_{m_α} . For an aircraft to be stable, $C_{m_\alpha} < 0$. Another important way to measure if an aircraft is longitudinally stable, is by determining the static margin, which is the distance between the neutral point of the aircraft and the center of gravity expressed as a percentage of the mean chord of the wing. The term, C_{m_α} , can be written as

$$C_{m_\alpha} = -C_{L_\alpha} K_n \quad (36)$$

where K_n is the static margin and C_{L_α} is the derivative of C_L with respect to α .

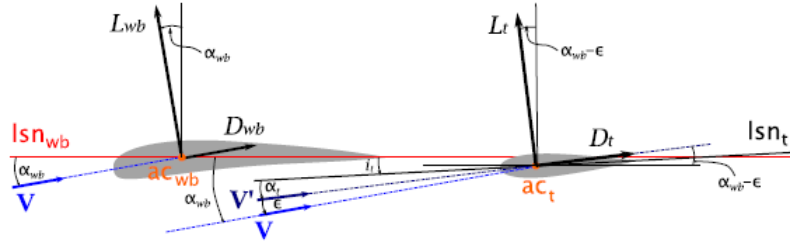


Fig. 40: Graphic representation of the lift forces on the wing and horizontal tail.

Using figure 40 as a reference, we can write that the total lift is the sum of the lift on the main wing plus fuselage (wb) and on the horizontal tail (t). As so, we can write the following

$$L = L_{wb} + L_t \implies \frac{L}{\frac{1}{2}\rho SV^2} = C_L = C_{L_{wb}} + \frac{S_t}{S} C_{L_t} \quad (37)$$

We can also assume a linear behaviour for these coefficients, $C_{L_{wb}} = a_{wb}\alpha_{wb}$ and $C_{L_t} = a_t\alpha_t$, where

$$\alpha_t = \alpha_{wb} - i_t - \epsilon \quad (38)$$

Taking the derivative of C_L , and after some manipulation, we get the following relation

$$C_{L_\alpha} \equiv a = a_{wb} \left[1 + \frac{a_t S_t}{a_{wb} S} (1 - \epsilon_\alpha) \right] \quad (39)$$

where a_{wb} and a_t is the derivative with respect to the angle of attack of the wing+fuselage and horizontal tail lift coefficients, respectively. The values for these terms were found using XFLR5 software, and are the following, $a_{wb} = 5.15666/\text{rad}$ and $a_t = 3.8388/\text{rad}$. S and S_t are the area of the main wing

and the horizontal tail, respectively, and ϵ_α is the derivative of the downwash angle with respect to the angle of attack. For this last parameter, figure 41 was used to estimate it. [25]

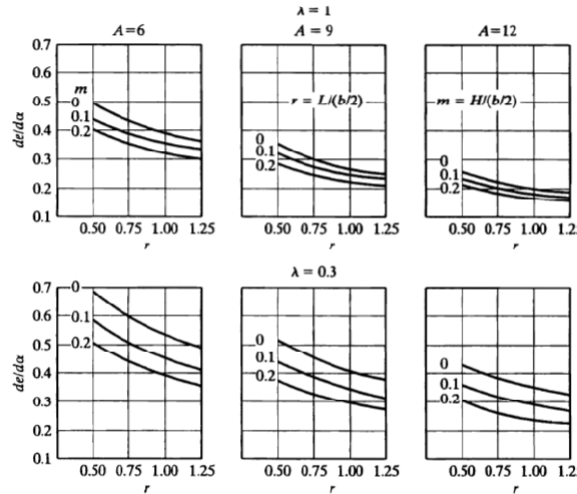


Fig. 41: Graphics showing the changes of ϵ_α .

As it can be seen, to estimate, we need some other parameters, such as the taper ratio, $\lambda = 0.4$, the factor $r = L/(b/2) = 0.8215$, where L is the distance between the aerodynamic centers of the main wing and horizontal tail, the main wing aspect ratio, $A = 6.55$, and the factor m which we will consider to be 0.

As it can be seen from figure 41, we do not have access to the graph with our exact values, therefore we will interpolate. Looking at the bottom left graph where $A = 6$ and $\lambda = 0.3$, increasing both these variables, there's a drop in ϵ_α . We will consider a value of $\epsilon_\alpha = 0.55$.

With the values previously found, we can calculate $C_{L\alpha} = 5.40325/\text{rad}$. Using the values previously shown in Table 37, and assuming that $h_n = 0.25$, we can calculate our static margin, $K_n = 0.0889 \Rightarrow 8.89\%$. Observing our static margin, we can note that the aerodynamic center is behind the center of gravity and that it is between the desired values (5% and 10%). This gives a value for $C_{m\alpha}$ of -0.3739/rad, which is negative, lying in the admissible range.

11.2 Lateral Stability

This type of stability, focus on the rolling motion of the aircraft. It describes its ability to come back to a neutral position when perturbed with a roll angle. The parameter we will be analysing is the derivative of the rolling moment coefficient with respect to the side slip angle, $C_{l\beta}$. For it to stable the following relation must be true, $C_{l\beta} < 0$.

For the term, $C_{l\beta}$, there are four big contributors: the dihedral angle and the leading edge angle of the main wing, the vertical tail and the main wing position.

$$C_{l\beta} = (C_{l\beta})_{\text{dihedral}} + (C_{l\beta})_{\text{lead. edge}} + (C_{l\beta})_{\text{vert. tail}} + (C_{l\beta})_{\text{wing pos.}} \quad (40)$$

The dihedral angle in our aircraft is 0, so its contribution is also null, $(C_{l\beta})_{\text{dihedral}} = 0$. The same applies to the leading edge angle contribution since $\Lambda = 0^\circ$. Therefore, $(C_{l\beta})_{\text{lead. edge}} = 0$.

Moving towards the vertical tail contribution, it can be written as

$$(C_{l\beta})_{\text{vert. tail}} = -a_F \frac{S_F z_F}{S_b} \quad (41)$$

where we can see that it depends on some wing's characteristics and the distance z_F , which is the vertical distance from the center of gravity and the aerodynamic center of the vertical tail. This parameter was found by doing an excel sheet where we introduced every component's vertical position with its masses, which gave us the vertical position of the center of gravity. For the vertical position of the aerodynamic center of the vertical tail the following equation was used, which gives us the position we want, starting from the wing root. [21]

$$z_{ac} = \frac{b}{6} \left(\frac{(1+2\lambda)}{1+\lambda} \right) = 0.8667m \quad (42)$$

Comparing it with the vertical position of the center of gravity, we get $z_F = 2.041m$. The contribution from the vertical tail is $(C_{l_\beta})_{vert. tail} = -0.0443/\text{rad}$.

Finally, for the contribution from the position of the wing, since our main wing is on top of the fuselage, its contribution is $(C_{l_\beta})_{wing pos.} = -0.00016^\circ = -0.009167/\text{rad}$. Adding all up, we get a value of $-0.05346/\text{rad}$ for C_{l_β} , and since it is negative, we are within the admissible range.

11.3 Direction Stability

For this stability study, we are focused on the yaw motion of our aircraft. It is the ability of the aircraft to come back to a neutral position, when perturbed with a yaw angle. The parameter in question is the derivative of the yaw moment coefficient with respect to the side slip angle, C_{n_β} . For it to stable the following relation must be true, $C_{n_\beta} > 0$.

For this derivative in question, we can assume that there is only one major contributor, the vertical tail. Its contribution can be written as the following

$$C_{n_\beta} = (C_{n_\beta})_{vert. tail} = a_F \frac{l_F S_F}{bS} \quad (43)$$

where we can see that it also depends on some wing's characteristics and the distance l_F , which is the longitudinal distance between the aircraft's center of gravity, and the vertical tail's aerodynamic center. For the aerodynamic center determination, it was assumed that the aerodynamic center of a simple airfoil is at a point located at 1/4 of the wings chord. Using this, we can calculate a value for $l_F = 4.122m$.

We can now calculate the derivative, and can in fact see that $C_{n_\beta} = 0.08946 > 0$, which is in the admissible range.

11.4 Vertical Stability

Finally, an additional analysis was made to reassure that the aircraft we defined, is vertically stable. This stability focus on the ability of the aircraft to pitch in both directions while flying vertically. This is very important for us, since our aircraft will take off vertically.

Our aircraft's center of gravity is located in a distance of 2.978m from the nose. Both pairs of rotors were said to be in a distance of 2.68m and 6.57m. Since the front rotors are in front of the center of gravity and the rear rotors are behind it, we conclude that we can generate both pitching motions from the force created by each pair of rotors. Analysing it more deeply, we can see that it was the fact that our leading edge was defined as zero that allowed us to push the front rotors forward.

The same analysis can be made laterally, by seeing if we can create both roll motions due to the propulsive forces. This analysis is somewhat obvious since the center of gravity is approximately in the center of the aircraft, $y \approx 0$, and we have rotors placed on both sides of the airplane. Therefore, we can conclude that the aircraft is vertically stable.

12 Aircraft Structures

This section will be focused on finding out the structural loads that the aircraft will be subjected to, during the different segments of the flight, normally due to the aerodynamic forces and the static and dynamic weight.

The V-n diagram will be analyzed for cruise altitude, as well as the shear loads and bending moments that the wing will support. It is normal to start with empirical analysis and progress to numerical high fidelity models as the project progresses from a conceptual design phase to further phases.

12.1 V-n Diagram

One of the diagrams that is used for structural analysis is the V-n diagram, which corresponds to the representation of the maximum expected loads that the aircraft will support, regarding the aircraft maneuvering capabilities and structural strength under various loading conditions, where the load factor, n , is plotted against the velocity of the aircraft.

The parameters needed for the next calculations are presented in following table.

Parameter	Value
$C_{L_{max}}$	1.73
C_{L_α} [rad]	5.51285
ρ [kg/m ³]	0.95697
W [N]	2378.8×9.81
S_w [m]	22.4
\bar{c} [m]	1.85

Tab. 38: Parameters for the V-n diagram calculations

The load factor is defined as the ratio between the lift and the weight:

$$n = \frac{L}{W} \quad (44)$$

In order to calculate the maximum load factor n_{max} , with MTOW expressed in lbs, an expression from EASA [19], was used:

$$n_{max} = 2.1 + \frac{24000}{MTOW + 10000} = 2.1 + \frac{24000}{2378.8 \times 2.205 + 10000} = 3.674 \quad (45)$$

From the n_{max} , we can obtain the n_{min} , by:

$$n_{min} = -0.4 \times n_{max} = -1.470 \quad (46)$$

To draw the V-n diagram, several velocities need to be calculated, such as the dive speed, stall speed, and others. From equation 45, it is possible to derive the following expression:

$$n = \frac{\frac{1}{2}\rho V^2 S C_{L_{max}}}{W} \Rightarrow V = \sqrt{\frac{2nW}{\rho S_w C_{L_{max}}}} \quad (47)$$

Taking into account that for the cruise altitude that the aircraft operates ($h = 2500$ m), the air density (ρ) is equal to 0.95697kg/m³, according to the "International Standard Atmosphere" (ISA).

The stall speed is obtained by considering $n = 1$, giving:

$$V_{Stall} = \sqrt{\frac{2 \times 2378.8 \times 9.81}{0.95697 \times 22.42 \times 1.73}} = 35.46 \text{m/s} \quad (48)$$

The maximum maneuvering velocity for positive lift, or the velocity at the flight condition of positive high angle of attack, is then calculated by considering $n = n_{max}$:

$$V_A = \sqrt{\frac{2 \times 3.674 \times 2378.8 \times 9.81}{0.95697 \times 22.42 \times 1.73}} = 67.969 \text{ m/s} \quad (49)$$

For the maximum airspeed that allows full maneuverability in a negative lift (point of the negative high angle of attack, assuming $C_{L_{max+}} = C_{L_{max-}}$), a velocity V_G is calculated, considering $n = n_{min}$:

$$V_G = \sqrt{\frac{2 \times 1.470 \times 2378.8 \times 9.81}{0.95697 \times 22.42 \times 1.73}} = 42.993 \text{ m/s} \quad (50)$$

As said before, the cruise velocity is equal to 212.4 km/h (59 m/s) for this case and for the dive speed, an approximation is made and $V_d = 1.5 \times V_{cr} = 88.5 \text{ m/s}$.

The results are summarized in the following table.

V_{Stall}	V_A	V_G	V_{cr}	V_d
35.46	67.969	42.993	59	88.5

Tab. 39: Relevant velocities (m/s) for the V-n diagram

As shown in the example in figure 42, the V-n diagram is divided by 3 main areas: the Stall Area, which is constrained by the aerodynamic limit and represents the region where a sudden reduction of lift occurs; the Flutter/Divergence Area, which is limited by both structural and operational limits, that represents the area where the structural damping is not sufficient to damp the induced vibration of the wind, amplifying vibrations and leading to structural failure (Flutter); and finally, the Operational Area, being constrained by the limits mentioned above.

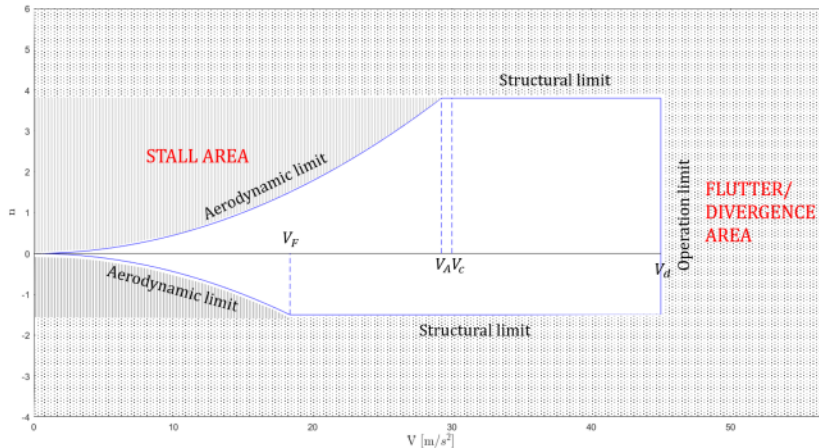


Fig. 42: Example of a V-n diagram

Now, taking into account the gust load factors, an analysis of the Gust Envelope will be done. Gust loads are produced by atmospheric perturbation and are considered unsteady aerodynamic loads, representing a load factor, that is now added to the ones calculated before.

These gusts will produce a change in the angle of attack, positive or negative, that will increase or decrease the lift, resulting in a change in the load factor, defined as $\Delta n = \frac{\Delta L}{W}$. Developing the expression, where the $n_{peak} = n + \Delta n$:

$$\Delta n = \frac{\rho u V C_{L\alpha} S}{2W} \quad (51)$$

The atmospheric turbulence occurs in many different frequencies, and so the aircraft will respond in many different ways. The frequency response of the aircraft is given in an equivalent way by the mass ratio μ :

$$\mu = \frac{2 \times \frac{W}{S}}{g \bar{c} \rho C_{L\alpha}} = 21.76 \quad (52)$$

This will influence the response coefficient K , calculated with:

$$K = \frac{0.88 \times \mu}{5.3 + \mu} = 0.70765 \quad (53)$$

As the values for the gust speed, \hat{u} , are based in statistical average from flight data (Fig. 43), they need to be corrected, and so,

$$u = K \hat{u} \quad (54)$$

Depending on the flight condition, different gust velocities will be considered. The statistical data used to calculate the gust velocities is shown in Figure 43. These values are shown in Table 40, already converted to m/s. u_1 is referred to v_a , which represents the Maximum Maneuvering Speed; u_2 is referred to v_c , which represents Cruise Speed; and finally, u_3 is referred to v_d , which corresponds to Dive Speed.

TABLE 10.3: Statistical gust velocity values.

Flight Condition	Altitude Range (f)	\hat{u} (f/s)	u_1	u_2	u_3
High Angle of Attack	0–20,000	66			
Level Flight	0–20,000	50			
Dive Condition	0–20,000	25			
High Angle of Attack	50,000	38	14.24	10.78	5.39
Level Flight	50,000	25			
Dive Condition	50,000	12.5			

Tab. 40: Gust Velocities

Fig. 43: Typical values for the gust velocities [6]

Applying all the expressions stated before, considering $n = 1$ and using equation (51), it is possible to obtain the values for this case, resumed in the following table.

$n \pm \Delta n$ (max)		$n \pm \Delta n$ (cruise)		$n \pm \Delta n$ (dive)	
3.468	-1.468	2.62	-0.62	2.22	-0.22

Tab. 41: Load factors accounting with the gust loads

The flight envelope is then represented in the next figure.

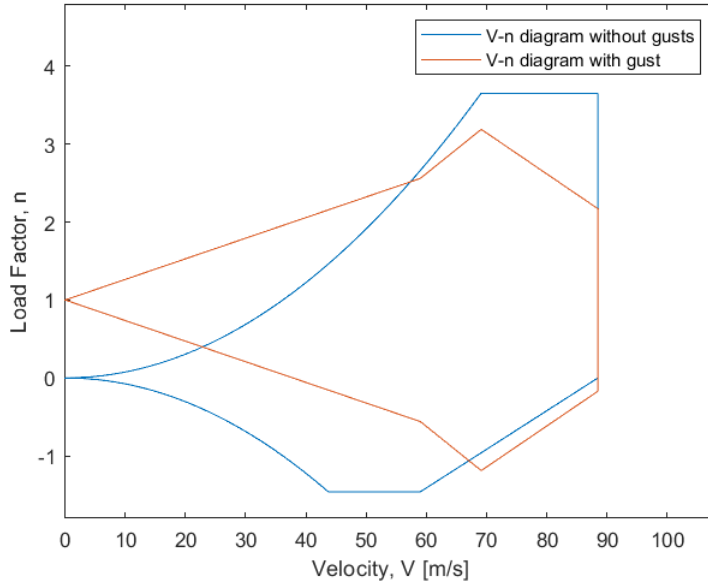


Fig. 44: Flight Envelope and Gust Envelope

To finish this analysis, the calculation of the design load factor is missing. First, the limit load factor is obtained, by considering the highest of all the maneuvering load factors plus the incremental load due to the gust.

$$n_{limit} = n_{max} + \Delta n = 3.674 + 2.468 = 6.142 \quad (55)$$

To obtain the n_{design} , the n_{limit} is multiplied by a safety factor, 1.5 (that is the normal value in the aircraft industry), to allow a safety margin in the structural design. This value represented the ultimate load that the internal structure will be able to support.

$$n_{design} = 1.5 \times n_{limit} = 9.213 \quad (56)$$

12.2 Wing Structural Analysis

One of the structures that handles part of the loads applied in the aircraft is the wing. In order to study the behavior of this component, as well as to calculate the structural load applied, an analysis will be done taking into account the loads due to the lift and wing weight.

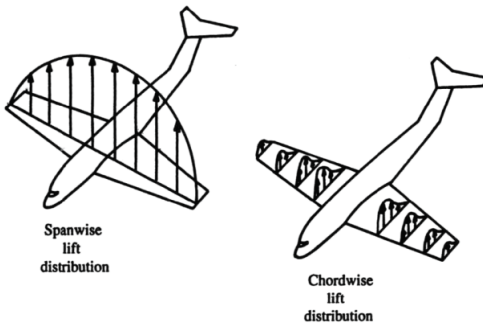


Fig. 45: Example of Loads in Lifting Surfaces

12.2.1 Lift Distribution

One of the loads that will act on the wing is the aerodynamic lift. In order to calculate the lift distribution along the wing span, and considering a trapezoidal wing, where L_r corresponds to the local lift at the wing root, the following expression is applied [6]:

$$L(y) = L_r \left[1 - \frac{2y}{b} (1 - \lambda) \right] \quad (57)$$

With some algebraic manipulation, it is possible to obtain the value of L_r and finally the expression for total lift distribution in the spanwise direction:

$$L_r = \frac{2L}{b(1 + \lambda)} \quad (58)$$

$$L(y) = \frac{2L}{b(1 + \lambda)} \left[1 - \frac{2y}{b} (1 - \lambda) \right] \quad (59)$$

The most important conclusion from this part of the work is to know what is the highest load that the wing will have to support, so the highest value of the lift load was calculated, the worst case scenario. For that, the design load factor, calculated in the previous section (Eq. 56), was used:

$$L = n_{design} \times W = 9.213 \times 2378.8 \times 9.81 = 214995\text{N} \quad (60)$$

Then, equation (59) comes:

$$L(y) = \frac{2 \times 214995}{12.1(1 + 0.4)} \left[1 - \frac{2y}{12.1} (1 - 0.4) \right] = 25383.1 - 2517.33y(\text{Nm}^{-1}) \quad (61)$$

12.2.2 Wing Weight Distribution

Another load that is important to consider is the wing weight. The first thing to do is to calculate an estimation for it. It was used the expression from [35], where $\Lambda_{1/2} = 0$, $W_0 = \text{MTOW} = 2378.8\text{kg}$, and $t_R = 0.12 \times 1.2 = 0.144$, which corresponds to the absolute value of thickness at the root of the wing:

$$\frac{W_{wing}}{W_0} = 0.0049(n_{design})^{0.55} \times \left[\frac{b}{\cos(\Lambda_{1/2})} \right]^{0.75} \times \left[1 + \sqrt{\frac{1.905 \cos(\Lambda_{1/2})}{b}} \right] \times \left[\frac{bS_w}{t_r W_0 \cos(\Lambda_{1/2})} \right]^{0.3} \quad (62)$$

$$W_{wing} = 333.954\text{kg} \quad (63)$$

Assuming a trapezoidal wing weight distribution, the same process used for the lift distribution can be applied here, resulting in the wing weight distribution of:

$$W(y) = \frac{2W}{b(1 + \lambda)} \left[1 - \frac{2y}{b} (1 - \lambda) \right] \quad (64)$$

$$W_{wing} = \frac{2 \times 333.954 \times 9.81}{12.1(1 + 0.4)} \left[1 - \frac{2y}{12.1} (1 - 0.4) \right] \quad (65)$$

$$W_{wing} = 386.788 - 38.359y(\text{Nm}^{-1}) \quad (66)$$

12.2.3 Shear Force and Bending Moments

With all the values for the loads acting at the wing calculated, and applying equation (68), it is obtained the shear force distribution, with W representing the sum of all loads acting on the wing.

$$V(y) = \int W dy \quad (67)$$

$$V(y) = \int_y^{b/2} (L(y) - W_{wing}(y)) dy \quad (68)$$

$$V(y) = 1239.5y^2 - 24996.3y + 105859(N) \quad (69)$$

For the bending moment, equation (70) is used, with V representing the shear force.

$$M(y) = \int V dy = \int_y^{b/2} (1239.5y^2 - 24996.4y + 105859) dy \quad (70)$$

$$M(y) = -413.17y^3 + 12498.2y^2 - 105859y + 274478(Nm) \quad (71)$$

Below, a representation of both shear force and bending moment across half of the wing can be seen in the respective figures 46 and 47, plotted in *MATLAB*.

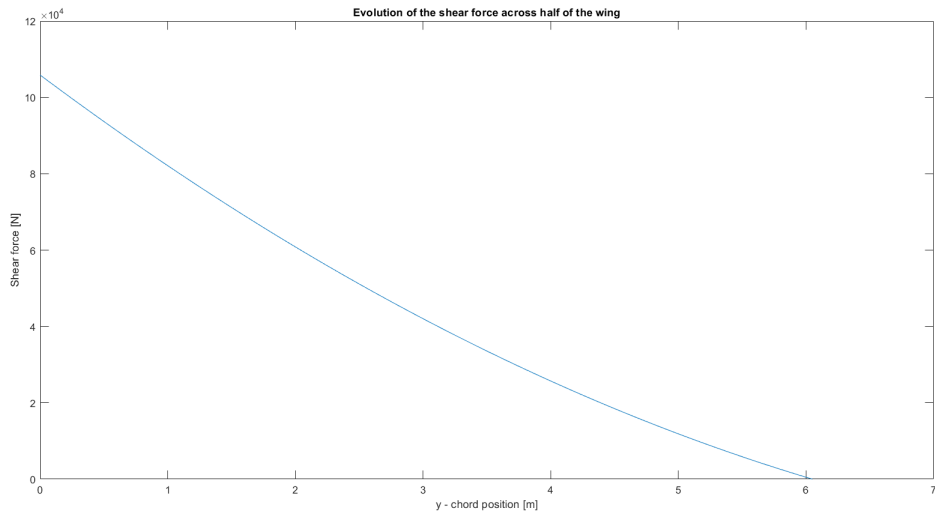


Fig. 46: Evolution of the shear force across half of the wing

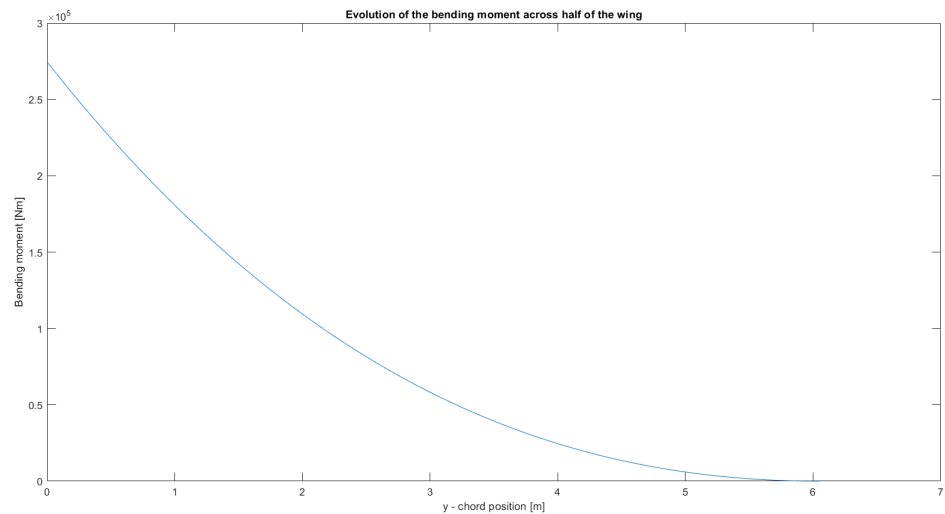


Fig. 47: Evolution of the bending moment across half of the wing

As it can be seen from the graphs, the maximum values for both shear force and bending moment occur at the root of the wing, as it was expected. For the shear force, a value of 105859N is obtained and for the bending moment 274478Nm is the obtained value.

13 CAD Design

The aircraft was modeled in the CAD software *NX Siemens*. The model goal is to combine all the parameters defined in the previous sections and make a visual representation of the aircraft.

In figure 48 we can find a CAD render of the aircraft, whilst in the following figures, 49, 50, 51, and 52, one can observe four views of the CAD model of the developed aircraft (isometric, top, side, and front, respectively).



Fig. 48: Model Render



Fig. 49: Isometric view



Fig. 50: Top view

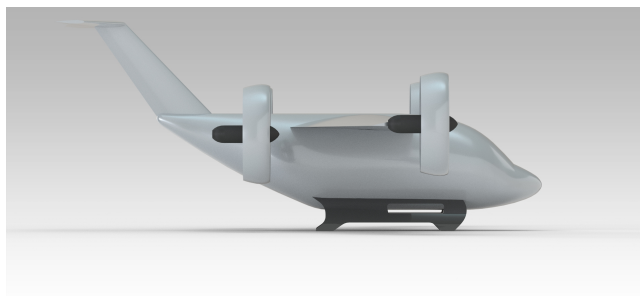


Fig. 51: Side view

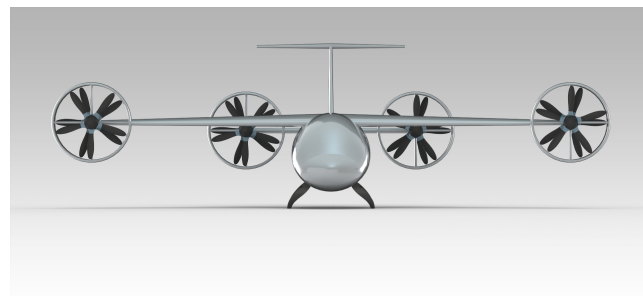


Fig. 52: Front view

14 Pollutant and Noise Emissions Estimations

14.1 Pollutant Emissions

Climate changes, global warming and air quality are major concerns from the community which are gaining relevancy in the past decades. Therefore, it is of the utmost importance to take these concerns into account right from the aircraft conceptual design stage. A commonly used metric is the Global Warming Potential (GWP) of the Life Cycle Assessment (LCA) methodology, where different emissions are expressed in a single metric: kilogram of CO₂ equivalent (kg CO₂-eq). Due to the unconventional nature of the Urban Air Mobility segment, information regarding aircraft production and end-of-life is either scarce or nonexistent. Thus only the emissions related to batteries and fuel are expected to be accounted for.

To proceed with the pollutant emissions study it is necessary, firstly, to know how much energy the fuel and the batteries provides to the aircraft. This is done by calculating the time of use of each energy source during the mission, taking in account the power needed for each phase of flight and the energy sources defined for each phase.

$$\begin{cases} \Delta t_{VTOL} = \Delta t_{verticalclimb} + \Delta t_{transition} + \Delta t_{verticaldescent} + \Delta t_{landing} = 255\text{s} \\ \Delta t_{forward} = \Delta t_{climb} + \Delta t_{cruise} + \Delta t_{descent} = 2848\text{s} \end{cases} \quad (72)$$

Now, using the values of power calculated in section X and the times calculated above, we can calculate the energy associated with each flight phase, VTOL (source of energy: battery) and forward flight (source energy: fuel).

$$\begin{cases} E_{bat} = P_{VTOL} \times \Delta t_{VTOL} = 816\text{KWh} \\ E_{fuel} = P_{forward} \times \Delta t_{forward} = 395\text{kWh} \end{cases} \quad (73)$$

In order to calculate the emissions generated by the aircraft, it is necessary to analyse the production and consumption cost of fuel and batteries, considering the cycles of battery life (the number of charge-discharge cycles a battery can withstand until it can no longer accept electrons). It is expected that the batteries will only be recharged in the end of the mission, meaning that the energy previously calculated corresponds to the energy provided during a cycle of charge-discharge.

When talking about the value for the number of cycles per life time, N_{cycles} , because we are using Li-ion batteries, we chose $N_{cycles} = 1000$. This value comes from the fact that this is the expectancy of achieve in the next years, when the aircraft is supposed to reach the market.

Concerning the emissions which result from the batteries production, the Li-ion batteries will produce $Emissions_{bat prod}^* = 147.7\text{kgCO}_2\text{-eq}/(\text{kWh})$. This value is very high, nevertheless this type of battery was chosen because we considered to be a better trade-off to use less batteries with high specific energy and high emissions than to use a less efficient type of battery as the production is an one-off event. Using this value and the energy that the battery supplies, we can calculate the emissions related to batteries production.

$$Emissions_{prod} = Emissions_{bat prod}^* \times E_{bat} = 8537\text{kgCO}_2\text{-eq} \quad (74)$$

Furthermore, it is assumed that batteries are going to be charged with energy from the electric grid, that has different pollution rates depending on the means used to produce energy, which vary from country to country. This is the value that will affect the consumption emissions of the batteries. For our case, the aircraft is operating in Japan, and the average emissions per unit of energy consumed was almost constant in the last years with a value $Emissions_{bat recharge}^* = 226.8\text{gCO}_2\text{-eq}/(\text{kWh})$.

Regarding the consumption of the fuel, although it can be expected that the pollution produced is similar to a car, the defined value is related to the internal combustion engine used. Nevertheless, no data was found about the model chosen, so it was assumed that $Emissions_{fuel c}^* = 0.0635\text{gCO}_2\text{-eq/MJ}$. Concerning the type of fuel, it was assumed that Jet Fuel A was the one used. The CO2-equivalent emissions per MJ of Jet Fuel A is $Emissions_{fuel prod}^* = 87.5\text{gCO}_2\text{-eq/MJ}$.

With this data, let us calculate the emissions associated to the use phase.

$$\begin{aligned} \text{Use Emissions per mission} &= Emissions_{bat recharge}^* \cdot E_{bat} + \\ &(Emissions_{fuel prod}^* + Emissions_{fuel c}^*) E_{fuel} = 111\text{kgCO}_2\text{-eq} \end{aligned} \quad (75)$$

The main difference regarding fuel and batteries emissions comes from the fact that fuel production must be taken into account for every cycle of charge-discharge, as it is burnt and reuse is not possible. With this, it can be stated that the total emissions per mission, excluding end-of-life emissions, is:

$$\text{Total Emissions per mission} = \frac{Emissions_{prod}^*}{N_{cycles}} + \text{Use Emissions per mission} = 119.54\text{kgCO}_2\text{-eq} \quad (76)$$

Comparing this value with the total emissions of a car (assuming that the car is more similar to our aircraft, than the train or the bus, for example, because those have preset routes), doing a mission with the same range (150km), at an average speed of 100km/h (the highest speed limit in Japan's highways), considering $P_{car} = 100\text{hp} = 74.57\text{kW}$ and the emissions related to the production and fuel consumption similar to the aircraft ones, the total emissions per mission is 35.3kgCO2-eq. This value is much smaller than the one obtained for our aircraft, although the mission duration is 1.5 hour for the car (definitely more because of the intense car traffic to get out of the city) and only 0.83 hour for the aircraft. Nevertheless, it is important to assume this problem and start to find solutions. A possible upgrade for our prototype is trying to use batteries as the only energy source. This is a market in expansion and the battery emissions are getting better every year. [32] [33]

14.2 Noise Emissions

As the aircraft that is being designed operates in urban areas, there is the need of evaluating other concerning factors. As so, noise estimations, as a topic of major importance, will be further analyzed. At first, the main objective was that the noise emissions in hover at 500ft did not exceed the value of 70dB.

Nevertheless, noise generation is still a difficult phenomenon to be predicted with accuracy. Semi-empirical models based on rotorcraft/helicopter data had to be used to provide the first estimation. In order to estimate the noise produced by the aircraft, rotational and vortex noises were considered. The program which was made available by the professors was used, and the value computed for maximum noise emissions near the ground was 79.516 dB.

Moreover, by testing the program with different inputs, it was clear that the factors that lead to higher noise emissions were the number of rotors, the rotational speed and the velocity of the tip. Nevertheless, even though the value of 79.516 dB was higher than what it was previously set as a goal, it was difficult, with these factors, to lower it.

The first iteration of the model considered a tip velocity of 240 m/s and the noise emission was estimated to a value above 80 dB. Although a reduction in the velocity of the tip did not change the noise emission value in a relevant manner, a reduction from 240 m/s to 230 m/s was enough to reduce the value to 79.516 dB. This reduction affected the design point, and, thus, a new iteration was made. The changes in the VTOL and Cruise phases were not significantly changed, and the motors installed can withstand the increased power needed, therefore we conclude that a tip velocity of 230 m/s is adequate to our concept aircraft.

Furthermore, even though the requirement of 70dB was not achieved, the value obtained for the SPL is acceptable, as it is within the limits of helicopters, which is set around 80dB. As so, the aircraft designed, as far as noise produced is concerned, is in advantage when compared to its biggest competitor. [32] [33]

15 Conclusion

15.1 Possible Improvements

In the final of any project it is very important to be critical and to see its strengths and flaws, so the group felt the necessity to write about the possible improvements that could be made to the developed concept.

The first improvement regards the airfoil profile. By using an already existent profile we could get an undesired downgrade in performance that could be avoided by using a personalized profile created with a genetic algorithm. This would create the perfect profile for the chosen mission.

The fuselage optimization is also an interesting aspect of the project that could be explored in the future. The group feels that the fuselage diameter could still be reduced and its shape explored in a more detailed way.

The choice of the aircraft materials was also an aspect of the project important to explore since it would bring some interesting challenges regarding both the weight optimization of the aircraft and its cost, for example.

Reducing the pollutant emissions by transforming the concept to an all electric aircraft is also an aspect to consider since the battery industry is in great expansion, and some years from now it could offer a more sustainable solution. Noise emissions could also be reduced by exploring the efficiency of the rotors, because the now estimated projection is slightly above 70dB, which is not ideal.

The aircraft transition to autonomous could be more explored, which is something which was not explored in detail. This transition would reduce the crew's mass and the operational costs, if implemented correctly.

The last improved suggested is regarding the costs estimation, both regarding the production and the operation. This would bring the debate about the viability about the use of this concept, and possibly the optimization of the mission itself.

These are just some of the improvements that could be made, which could be useful for the future if this concept would advance to its next stage of development.

15.2 Final Remarks

Projecting a concept in UAM presented a lot of challenges since it is an area which is in the first stages of development. So the research regarding what was already done was difficult, which gave the group a lot of freedom during the process, and implied a lot of creativity and critical spirit to reach both an innovative and possibly functional design. However, because of this lack of information, the project could have some fundamental flaws regarding its design, which is usual during this concept phase and expected to be corrected deeper within the project. Sadly, this project could only move forward, and even be used in other type of applications, different from the mission presented, if it had access to investment, which is unlikely.

References

- [1] 228 (109kW / 230Nm). (2022, May 9). EMRAX. <https://emrax.com/e-motors/emrax-228/>
- [2] 268 (200kW / 500Nm). (2022, May 9). EMRAX. <https://emrax.com/e-motors/emrax-268/>
- [3] Bell Nexus 6HX. (2022, May 9). https://evtol.news/__media/Aircraft%20Directory%20Images/Bell%20Nexus%206HX/Bell-Nexus-image-15-1.jpg
- [4] Bell Nexus 6HX. (2022, May 9). <https://www.bellflight.com/products/bell-nexus>
- [5] Broutier, J. (n.d.). Pratt & Whitney Canada PT6B-9. Aircraft Database. Retrieved May 22, 2020, from <https://aircraft-database.com/database/engine-models/pt6b-9>
- [6] Corke, T. (2002). *Design of Aircraft* (1st ed.). Pearson.
- [7] Equipmake. (2021, August 31). APM-200. <https://equipmake.co.uk/products/apm-200/>
- [8] Equipmake. (2022, May 26). APM-120. <https://equipmake.co.uk/products/apm-120/>
- [9] European Aviation Safety Agency. (2010, Aug 19). Honeywell International Inc. LTS101 series engines. Retrieved from [https://www.easa.europa.eu/sites/default/files/dfu/EASA-TCDS-E-228_\(IM\)_Honeywell_International_Inc._LTS101_series_engines-04-19082010.pdf](https://www.easa.europa.eu/sites/default/files/dfu/EASA-TCDS-E-228_(IM)_Honeywell_International_Inc._LTS101_series_engines-04-19082010.pdf)
- [10] European Aviation Safety Agency. (2015, Oct 06). Retrieved from Pratt and Whitney Canada PW206 and PW207 series engines. Retrieved from <https://www.easa.europa.eu/downloads/7769/en>
- [11] Eve, Mobility Reimagined. (2022, May 9). <https://eveairmobility.com/>
- [12] Gudmundsson, S. (2014). General Aviation Aircraft Design: Applied Methods and Procedures. Elsevier.
- [13] Honeywell. (2019, Feb). 200 kW Power Generation. Retrieved from https://aerospace.honeywell.com/content/dam/aerobt/en/documents/learn/products/electric-power/brochures/N61-2024-000-000_200kw-Generator_v2.pdf
- [14] Introducing the first electric vertical take-off and landing jet. (2022, May 9). <https://lilium.com/jet>
- [15] Leishman, G. J. (2006). *Principles of Helicopter Aerodynamics* (2nd ed.). Cambridge University Press.
- [16] Lilium Jet. (2022, May 9). <https://imageio.forbes.com/specials-images/imageserve/602351a5bbd211f5f4df8c26/Lilium-jet/1960x0.jpg?format=jpg&width=960>
- [17] Lycoming LTS101-850B-2. (n.d.). Helis.Com. <https://www.helis.com/database/engines/LTS101-850B-2/>
- [18] Maker 101. Introducing Maker. (2022, May 9). <https://www.archer.com/maker>
- [19] Maximum manouevring load factor, (accessed from May 30, 2022). <https://www.easa.europa.eu/sites/default/files/dfu/CS-23%20Initial%20issue.pdf>.
- [20] Norton, R. L. (2010). *Machine Design: An Integrated Approach* (4th ed.). Pearson.

- [21] Raymer, D. P. (2002). Aircraft Design: A Conceptual Approach. AIAA (American Institute of Aeronautics & Astronautics).
- [22] Rolls Royce. (2009, May). *RR500 Turboprop*. Retrieved from <https://www.experimentalaircraft.info/doc/turbines/rr500-specs.pdf>
- [23] Rolls-Royce EVTOL. (2022, May 9). https://evtol.news/_media/Aircraft%20Directory%20Images/Rolls-Royce%20EVTOL/rolls-royce-evtol-in-flight.jpg
- [24] *Rolls-Royce powered concepts.* (2022, May 9). <https://www.rolls-royce.com/products-and-services/electrical/propulsion/air-taxis.aspx>
- [25] Silverstein Abe, Katzoff S, *Design charts for predicting downwash angles and wake characteristics behind plain and apped wings*, United States, 1939 January, NACA-TR-648
- [26] Suleman, A. *Lecture Notes: Lecture 5 - Tail Design*, 2022.
- [27] Suleman, A. *Lecture Notes: Lecture 6a - Airfoil Selection*, 2022.
- [28] Suleman, A. *Lecture Notes: Lecture 6b - Wing Design*, 2022.
- [29] Suleman, A. *Lecture Notes: Lecture 7 - Propulsion*, 2022.
- [30] Suleman, A. *Lecture Notes: Lecture 7 - Propulsion - Tilt-rotor Example*, 2022.
- [31] Suleman, A. *Lecture Notes: Lecture 8 - Fuselage Design*, 2022.
- [32] Suleman, A. *Lecture Notes: Lecture 12 - Pollutant and Noise Emissions*, 2022.
- [33] Suleman, A. *Lecture Notes: Lecture 12 - Pollutant Emissions - Tilt-rotor Problem*, 2022.
- [34] Tacke et al. *World Directory of Light Aviation* 2015-16, pages 262-263. Flying Pages Europe SARL, 2015. ISSN 1368-485X
- [35] Torenbeek E. "Synthesis of subsonic airplane design", 1982. <http://resolver.tudelft.nl/uuid:229f2817-9be9-49b6-959a-d653b5bac054>
- [36] *Uber Elevate eCRM-001*. (2022, May 9). <https://evtol.news/uber-elevate-ecrm-001/>
- [37] Weden, G. J., & Coy, J. J. (1984, October). *Summary of Drive-Train Component Technology in Helicopters*. NATO-AGARD PEP Sixty-fourth Symposium on Gears and Power Transmissions for Helicopters and Turboprops, Lisbon, Portugal.